

Detached Red Giant Eclipsing Binary Twins: Rosetta Stones to the Galactic Bulge

Nataf, D. M.

Department of Astronomy, Ohio State University, 140 W. 18th Ave., Columbus, OH 43210
nataf@astronomy.ohio-state.edu

Gould, A.

Department of Astronomy, Ohio State University, 140 W. 18th Ave., Columbus, OH 43210
gould@astronomy.ohio-state.edu

Pinsonneault, M. H.

Department of Astronomy, Ohio State University, 140 W. 18th Ave., Columbus, OH 43210
pinsono@astronomy.ohio-state.edu*Received March 24th, 2012***Abstract**

We identify 34 highly-probable detached, red giant eclipsing binary pairs among 315 candidates in Devor's catalog of $\sim 10,000$ OGLE-II eclipsing binaries. We estimate that there should be at least 200 such systems in OGLE-III. We show that spectroscopic measurements of the metallicities and radial-velocity-derived masses of these systems would independently constrain both the age-metallicity and helium-metallicity relations of the Galactic Bulge, potentially breaking the age-helium degeneracy that currently limits our ability to characterize the Bulge stellar population. Mass and metallicity measurements alone would be sufficient to immediately validate or falsify recent claims about the age and helium abundance of the Bulge. A spectroscopic survey of these systems would constrain models of Milky Way assembly, as well as provide significant auxiliary science on research questions such as mass loss on the red giant branch. We discuss the theoretical uncertainties in stellar evolution models that would need to be accounted for to maximize the scientific yield.

Galaxy: Bulge – Galaxy: stellar content – binaries: eclipsing

1. Introduction

To understand the origin and evolution of the Galactic Bulge, one would like to measure the age, kinematics, and abundances for a large and representative sample of stars. Because both photometric and spectroscopic ages are strongly degenerate with helium abundance (Marín-Franch *et al.* 2010; Nataf & Gould 2011), it is absolutely essential that each star in such a sample have an estimate of its helium content, in addition to the “metal” abundances that are more usually reported. This appears to be a daunting requirement: despite the fact that helium comprises 25–40% of the baryonic mass of Bulge stars, there are no reported spectroscopic helium estimates, other than that of the stripped B-star S2 orbiting the supermassive black hole at the center of our Galaxy (Martins *et al.* 2008). Helium is simply too tightly bound to give rise to detectable lines in the relatively cool stars that inhabit the Bulge, though the application of Herculean techniques to the HeI 10830 has shown promise in the case of the metal-poor globular cluster NGC 2808 (Pasquini *et al.* 2011).

Here we argue that well-detached double-red-giant eclipsing binaries can provide a large $O(10^2)$ sample of such well-characterized stars. The choice of double-red-giant eclipsing binaries is far from obvious. Red giants (RGs) of luminosity comparable to the red clump (RC) are themselves relatively rare, roughly one per $10^3 M_\odot$. And it is straightforward to show that only $O(10^{-5})$ of these have detached eclipsing secondaries of comparable size. So, for example, one does not expect even one such binary in the entire system of Milky Way globular clusters. Detached eclipsing turnoff stars are at least 1000 times more plentiful. However, these systems do exist and are accessible once one has access to photometric surveys as large as OGLE: We note the recent detailed investigation of $3.5 M_\odot$ RG twins in a 371.6 day orbit, OGLE SMC113.3 4007 (Graczyk *et al.* 2012).

Nevertheless, for the specific problem of tracing the Bulge population, double-RG eclipsing binaries are very much preferred. The principal reason is simply that they are brighter and hence all measurements are much more precise given instrumentation available currently or in the foreseeable future. For example, currently it is possible to obtain detailed spectroscopic abundances for turnoff stars only when they are highly magnified (Bensby *et al.* 2010, 2011). For the same reason, precision radial velocity (RV) measurements, needed for accurate masses, are extremely costly for turnoff stars. Even photometric light curves, which are required to measure the mean density of the system, are challenging (e.g. Clarkson *et al.* 2011). This is not just because of the low flux levels of the source but more fundamentally, irreducible blending by ambient stars, as well as third bodies that are frequently present in close-binary systems (Tokovinin *et al.* 2006; Pribulla & Rucinski 2006). Finally, because the Bulge has finite depth ($\sigma_{(m-M)_0} \sim 0.15$ mag) and is subject to differential extinction, one cannot, in strong contrast to globular clusters, use photometric information to precisely determine the phase of stellar evolution of a given turnoff star.

All of these problems are greatly reduced in RGs. Plentiful photons easily yield high signal-to-noise ratio (S/N) measurements. Blending is intrinsically less important because the sources are bright, and moreover it is possible to detect blends down to very low flux levels. High flux levels and low-blending imply that proper motions are more precisely measured, and precise lightcurves enable accurate distance measurements using standard eclipsing-binary techniques (at least to determine relative positions within the Bulge). Finally, the whole phase of RG evolution is short, so that the phase of stellar evolution can be determined extremely precisely. The only real problem is the low frequency of detached double-red-giant eclipsing binaries. However, in this Paper we show that at least 34 such systems are already present in the eclipsing-binary catalog constructed by Devor (2005) from OGLE-II data.

The structure of this paper is as follows. In Section ??, we show how to identify Galactic bulge RG EB twins from an order of magnitude larger list of candidates. The observed frequency of these systems in OGLE-II implies that there are of order 200 more waiting to be discovered in OGLE-III data. In Section ??, we summarize the stellar models used in this work. In section ??, we discuss the immediate science that could be achieved with even preliminary spectroscopic follow-up. We find that mass and metallicity measurements would, by themselves, be sufficient to validate or falsify several hypotheses of the Bulge stellar population. In Section ??, we investigate how well the system parameters must be measured and how the precision of these measurements translate into errors on the age-helium plane. Further, we show that if current theoretical and observational uncertainties on the RG temperature scale are reduced in the future, and if tidal effects could be taken into account by either selecting very detached systems or effectively modelling them, detached RG eclipsing binaries could in and of themselves be sufficient to fully characterize the Galactic Bulge age-helium-metallicity relationship.

2. At Least 34 Detached Red Giant Eclipsing Binary Pairs in the OGLE-II Eclipsing Binary Catalog

There are significant challenges in finding RG eclipsing binary pairs. First, the lifetime of the RG phase is only $\sim 1\%$ of the stellar lifetime, which means that the two masses can differ by no more than $\sim 0.5\%$ for both stars to be in the RG phase simultaneously. Second, from Kepler's third law:

$$\left(\frac{a}{10R_{\odot}}\right) = 0.84 \left(\frac{P}{2 \text{ days}}\right)^{2/3} \left(\frac{M_1 + M_2}{2M_{\odot}}\right)^{1/3}, \quad (1)$$

it follows that RG eclipsing binary pairs will not be detached for the short orbital periods that are the most easily detected, due to their large physical size. Meanwhile, at longer periods, the geometrical probability of eclipse will go down as the inverse of the orbital separation, and even for fortuitous alignments for which

$\sin i \sim 1$, the S/N will drop sharply with increased orbital separation as there will be fewer completed periods to phase the lightcurve over.

It is therefore not surprising that a photometric database as large as that of OGLE is required to produce a catalog of these systems. Devor (2005) combed through 218,699 variable stars in the OGLE-II Bulge photometric survey, to identify 10,862 eclipsing binaries. There were 3,170 classified as detached eclipsing binaries, the overwhelming majority of which are foreground main-sequence disk stars. The top-left panel of Figure Fig. 1 shows the dereddened color and magnitude of the 3,170 detached eclipsing binaries overplotted on a dereddened OGLE-III CMD of Baade’s window (Szymański *et al.* 2011). Only 315 of the catalog members have dereddened color $(V - I)_0 \geq 0.7$ and $P \geq 2$ days.

Though each of these candidates appear as RGs on the CMD and have eclipsing binary lightcurves, many are not true RG eclipsing binaries. We find that at least 33 of these 315 candidates have unphysical parameters, as determined by deriving radius estimates. The solutions of Devor (2005) include the orbital periods and the ratios $R_{1,2}/a$, allowing estimates of the primary’s physical radius, $r = 5.30R_\odot(r_1/a)(P/\text{days})^{2/3}$, where we have assumed $M_1 + M_2 = 2M_\odot$. This assumption of the mass will not contribute significant error due to the small value of the exponent: $1/3$. An independent estimate of the radii of these stars can be derived photometrically, by dereddening their colors and magnitudes assuming an intrinsic color and brightness of the red clump (RC) $(V - I, I)_{RC} = (1.06, -0.10)$, $(m - M)_{0,\text{Bulge}} = 14.52$ and using the empirical color-surface-brightness relations of Kervella *et al.* (2004), by first transforming $(V - I)$ to $(V - K)$ using the *VIK* color-color relation of Bessell & Brett(1988). The results of this comparison are shown in the bottom panel of Figure Fig. 1. There is a sequence of sources, plotted in blue, for which the ratio $R_{\text{orbit}}/R_{\text{photometric}}$ reaches values as high as 10. These are manifestly unphysical, and they comprise $\sim 10\%$ of the eclipsing-binary candidates with $(V - I)_0 \geq 0.7$ and $P \geq 2$ days. That these form a sequence strongly implies that they are a specific class of variables that happen to strongly resemble eclipsing binaries. We note that they are all as bright or brighter than the RC.

The 34 red points, which we call the “gold sample”, have a minimal size criterion $R_{\text{secondary}} \geq 3R_\odot$ (to ensure that both members are RG stars), and a consistent size criterion $|\log(R_{\text{primary,orbit}}/R_{\text{primary,photometric}})| \leq 0.10$, equivalent to a $\sim 25\%$ error in the radius or 0.5 mag in the brightness. This is an estimate of the effects due to errors in the corrections between color and surface brightness, differential reddening, and depth relative to the Galactocentric distance. 248 of the candidates, plotted in green, have properties that are physical but not optimal. Many are likely disk stars, other may have secondaries on the subgiant branch, for which follow-up analysis would not be able to assume $M_1 = M_2$. We classify these as the “silver” sample. We directly inspected each of the 34 gold eclipsing binary lightcurves by downloading photometry from the OGLE-II archive (Udalski *et al.* 1997; Szymański *et al.* 2005). The OGLE-II lightcurves for the gold-sample candidates are

shown in Fig. 2, 3, and 5. Both “gold” and “silver” candidates are listed in Tables 1 and 2.

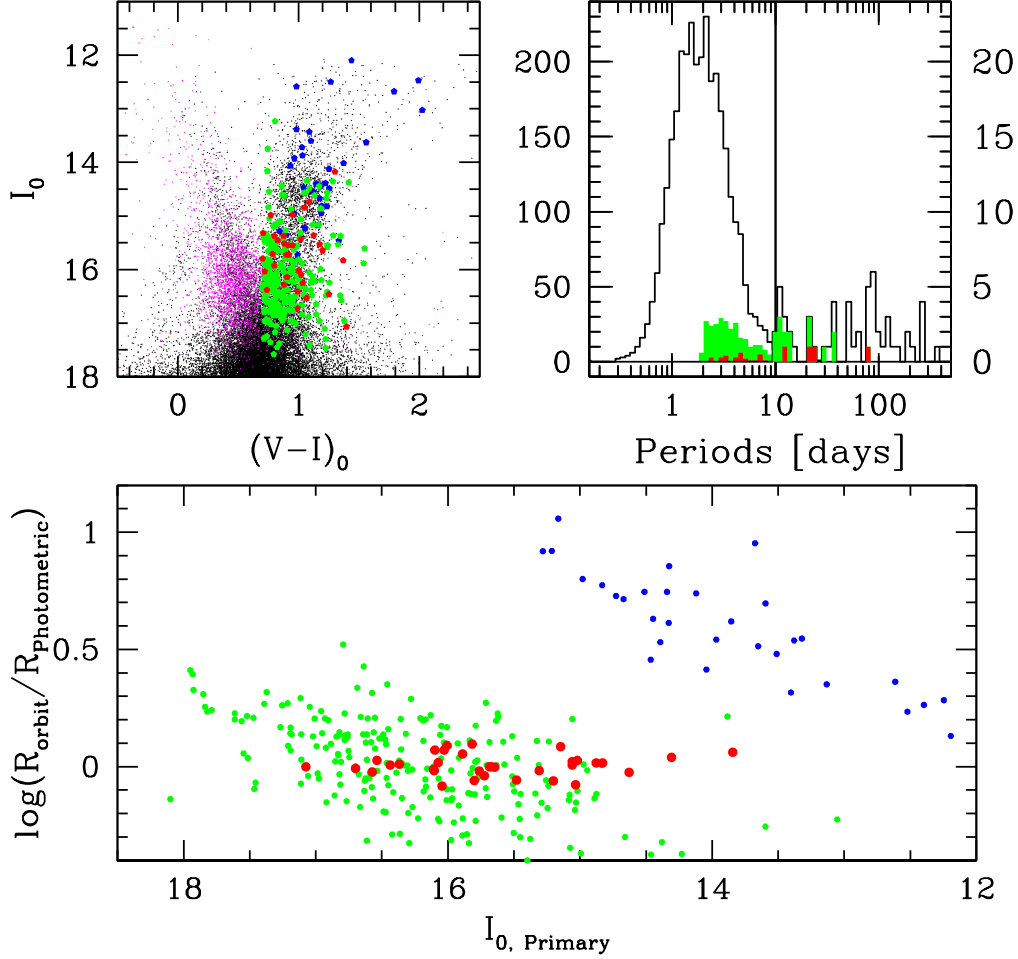


Figure 1: At least 34 of the 10,862 OGLE-II eclipsing binary candidates in the catalog of Devor (2005) are detached RG eclipsing binary pairs. TOP-LEFT: Dereddened color and magnitude of detached binaries (magenta), “gold”, “silver”, and spurious eclipsing binary sources with $(V - I)_0 \geq 0.7$ and $P \geq 2$ days (red, green, blue respectively), overplotted on a dereddened OGLE-III CMD toward Baade’s window (black). TOP-RIGHT: Histogram of period distribution of 3,177 detached eclipsing binaries, with the distribution of periods greater than 10 days enlarged. BOTTOM: Comparison of stellar radii derived from the photometric and orbital information for the primary stars as a function of $I_{0, \text{Primary}}$. Same color scheme as top-left. The gold candidates pass the test of having consistent radii from photometry and orbital parameters.

There may be more such systems to be found at brighter magnitudes. It has been demonstrated that there is a substantial population of undiscovered, bright periodic variables toward the Galactic Bulge. However, OGLE photometry, from which the eclipsing binary candidates are derived, saturates at $I \sim 13$ (Szymański *et al.* 2005). Nataf *et al.* (2009), as part of a microlensing feasibility study investigating bright ($8 \lesssim I \lesssim 13$) stars toward the Galactic Bulge, took 151 exposures spanning 88 nights and estimated that 50% of the periodic variables were not previously detected. Due to the short baseline, it is not surprising that no long-period detached eclipsing binaries are present in the catalog of 52 previously undetected eclipsing binaries (Nataf *et al.* 2010), but it is likely that a few could be found near the tip of the RG branch by a dedicated campaign with a small-aperture telescope.

2.1. Uncertainties in the Photometric Parameters

We comment on a few uncertainties in the parameters derived by Devor (2005) and how they can be rectified.

The first is that of ellipsoidal variations, which are not accounted for. Ellipsoidal variations result from the geometric distortion of close eclipsing binary stars due to their mutual gravitation. That this was not taken into account by Devor (2005) likely results in small errors in some of the parameters such as the stellar densities. However, this effect could be well approximated for in a more detailed study. From Equation (6) of Morris (1985), the mean magnitude difference between maxima and minima resulting from ellipsoidal variations, ΔM , behaves as:

$$\Delta M = 0.325 \frac{(\tau_1 + 1)(15 + \mu_1)}{(3 - \mu_1)} \left(\frac{m_2}{m_1} \right) \left(\frac{R_1}{a} \right)^3 \sin^2 i, \quad (2)$$

where μ_1 is the primary's linear limb-darkening coefficient and τ_1 is the primary's gravity-darkening coefficient. From Table 1 of Al-Naimiy (1978), we find $\mu_1 \sim 0.6$, and $\tau_1 \sim 0.4$ from Al-Naimiy (1978) and Equation (10) of Morris (1985), where we assume 4000 K objects measured at 8000 Å for both parameters. For edge-on RG EB twins, $(m_2)/(m_1)\sin^2 i \sim 1$, and thus Equation ?? reduces to:

$$\Delta M \approx 2.96 \left(\frac{R_1}{a} \right)^3 = 0.024 \left(\frac{R_1/a}{0.2} \right)^3, \quad (3)$$

which corresponds to the typical between-eclipse trends seen in Fig. 3, 4, and 5.

Some readers may be concerned about a possible factor of 2 degeneracy in the period calculation: Devor (2005) assumes there are always two measurable eclipses. We argue that this is a valid assumption for these stars. First, with their position on the Bulge CMD and the match between their photometric and orbital radii, we are confident that these are RG stars. Second, the eclipse depths seen in Fig. 3, 4, and 5 range from 0.1 to 0.4 mag. It is difficult to conceive of a plausible object that could eclipse $\sim 30\%$ of a RG's light and not be a RG itself, at which point two eclipses would be inevitable.

The third source of error is that of the eclipse phase. Observers may wish to know the phase of the orbit to optimize their RV targeting, for example by obtaining the spectra during the secondary eclipse, when the smaller RG is fully obscured by the larger RG, an epoch we label E_2 . Unfortunately, knowledge of the period phases is now somewhat lost, since OGLE-II observations (Udalski *et al.* 1997; Szymański *et al.* 2005) were taken in the period 1997-2000, and typical periods for these sources is 20 days. Additionally, many of our values of E_2 may be off by $\sim P/2$ if the photometric fit incorrectly determined the surface brightness ratio of the two stars. This phase drift will be easy to account for once time-series photometry from the OGLE-III survey (Szymański *et al.* 2011) become available, as these will allow tighter period determinations and cover the time baseline 2002-2009.

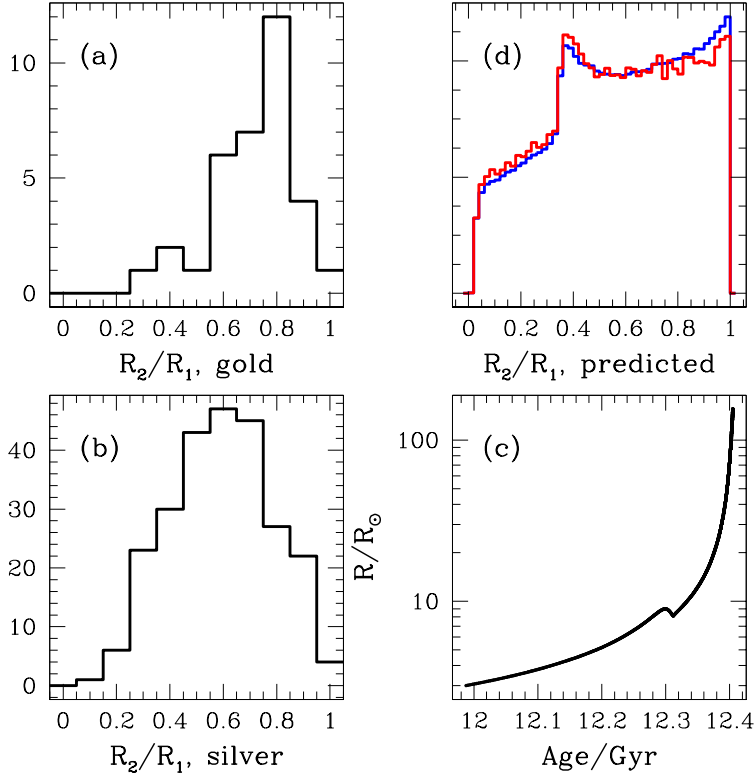


Figure 2: The observed distribution of R_2/R_1 does not match simple expectations, suggesting selection effects. **Panel (a)** R_2/R_1 for the 34 gold sample EB systems. **Panel (b)** R_2/R_1 for the 248 silver sample EB systems. **Panel (c)** A solar chemistry, $1 M_\odot$ stellar track computed using the Yale Rotating Stellar Evolution Code (YREC, Delahaye *et al.* 2010), we show the track for $R \geq 3R_\odot$, up to the tip of the RG branch. **Panel (d)** Predicted R_2/R_1 for any binary RG twin sampling the probability density function from Panel c (blue), and predicted R_2/R_1 for detached binary RG twins modified to account for the period distribution of Duquennoy & Mayor (1991), and assuming an eclipse probability $(R_1 + R_2)/a$.

2.2. Biases in the Sample of Devor (2005)

We compare our derived distribution of R_2/R_1 for both the gold and silver samples, shown in panels (a) and (b) of Fig. 2, and we find that these are not consistent with expectations: the catalog is likely missing RG EB twins with both high and low radius ratios. The expected probability density functions for R_2/R_1 are derived by sampling a scaled-solar stellar track (Delahaye *et al.* 2010, see Section ??) in the evolution phase during which $R \geq 3R_\odot$ but before the tip of the RG branch (mimicking our selection for the gold sample). Due to the fact that the mass difference for equal metallicity and co-eval stars on the RG branch is small, it follows from

the fuel-consumption theorem (Renzini & Buzzoni 1986) that the relative number counts are simply proportional to the duration of specific phases of stellar evolution, in this case:

$$N(r)dr \propto \tau(r)dr. \quad (4)$$

We randomly sample the stellar track in age (equivalent to sampling in phase) 2×10^6 times, and in panel (d) of Fig. 2 we show (in blue) the resulting distribution of R_2/R_1 . We also show a corrected predicted probability density function (in red) that accounts for the empirical period distribution of Duquennoy & Mayor (1991) given the assumption that $M_1 = M_2 = 1M_\odot$, the requirement that the EBs be detached, and the assumption of an eclipse probability $P(E) = (R_1 + R_2)/a$. The ratio of R_2/R_1 is predicted to increase smoothly, approximately doubling, over the range $0 \leq R_2/R_1 \leq 1$, with an excess at $R_2/R_1 \sim 0.45$ due to the red giant branch bump (RGBB). Instead, both the gold and silver sample peak at $R_2/R_1 \sim 0.75$, with a sharp dropoff at both ends.

We suggest two plausible reasons for the difference between the observed and predicted distributions of R_2/R_1 . At low values of R_2/R_1 , the photometric eclipse depth drops rapidly, and thus may evade detection by the algorithm of Devor (2005). At high values of R_2/R_1 , the eclipses may become identical in shape, a solution that may be indirectly biased against by the detection algorithm. We argue against the RC playing a significant role in these biases. It is not included in our predicted luminosity function, but as can be seen in the top left panel of Figure Fig. 1, very few of the EB twins (either gold or silver) are in the RC. There is a sound theoretical reason to expect this. All RC stars will have previously ascended the RG branch and reached very high values of R/R_\odot . Thus, if they have a binary companion sufficiently close as to have detectable eclipse once their size shrinks to $R \approx 10R_\odot$, they would have significantly overflowed their Roche lobes, and thus likely ended up on a section of the zero-age horizontal branch corresponding to higher mass-loss.

Due to the biases in the sample, we cannot assess whether our assay is consistent with the claim that close binaries have a flat secondary mass function, a result observed for various types of binary stars (Kuiper 1935; Pinsonneault & Stanek 1996). If the detection efficiency is far below 100%, then our estimate of 200 ‘‘gold’’ candidates waiting to be found in OGLE-III data is an underestimate. We derived this number by taking the 34 candidates found in OGLE-II and scaling by the ratio (~ 6) of Bulge RR Lyrae found in OGLE-III (Soszyński *et al.* 2011) to that found in OGLE-II (Collinge *et al.* 2006). However, if RG EB twins in OGLE-II had a low detection efficiency, the benefit of using the higher-cadence, longer-baseline, and more precise OGLE-III data will be substantially higher than naively estimated.

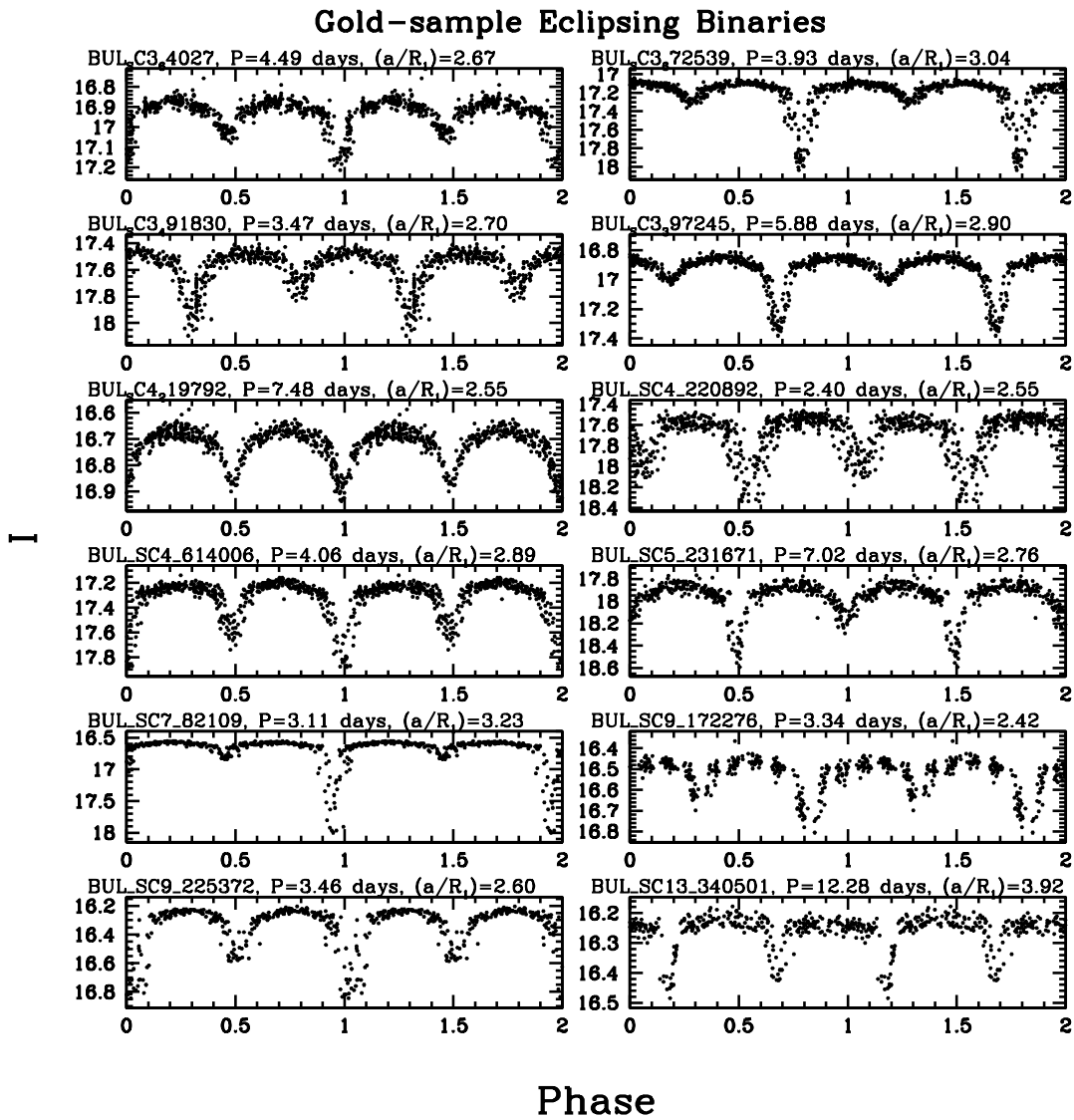


Figure 3: OGLE-II photometry (Udalski *et al.* 1997; Szymański *et al.* 2005) for gold-sample eclipsing binary stars phase-folded over the periods measured by Devor (2005). For each binary we state the OGLE-II identification, as well as the period and ratio of semimajor axis to primary radius measured by Devor (2005).

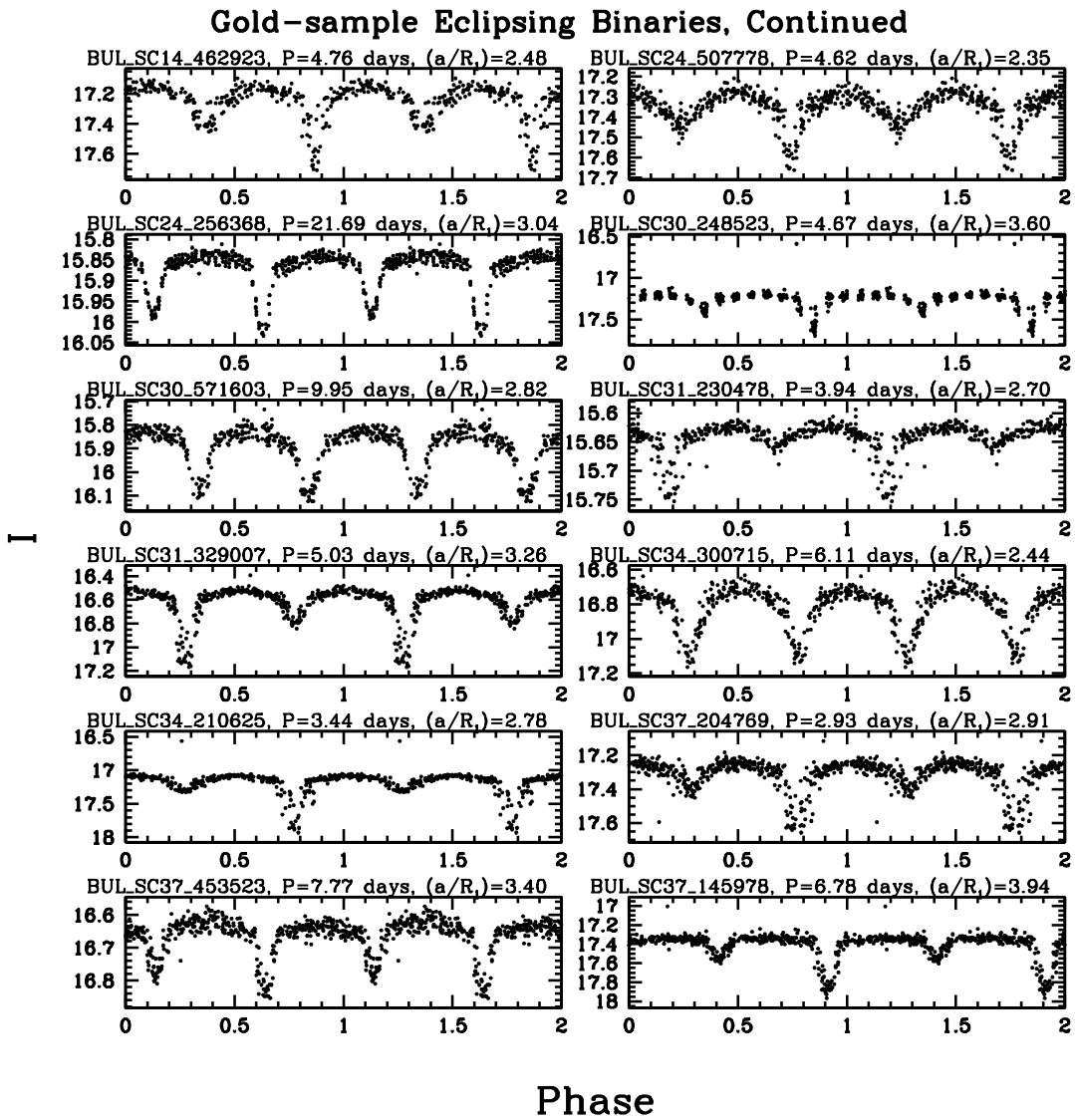


Figure 4: Same as in Fig. 3.

Gold-sample Eclipsing Binaries, Continued

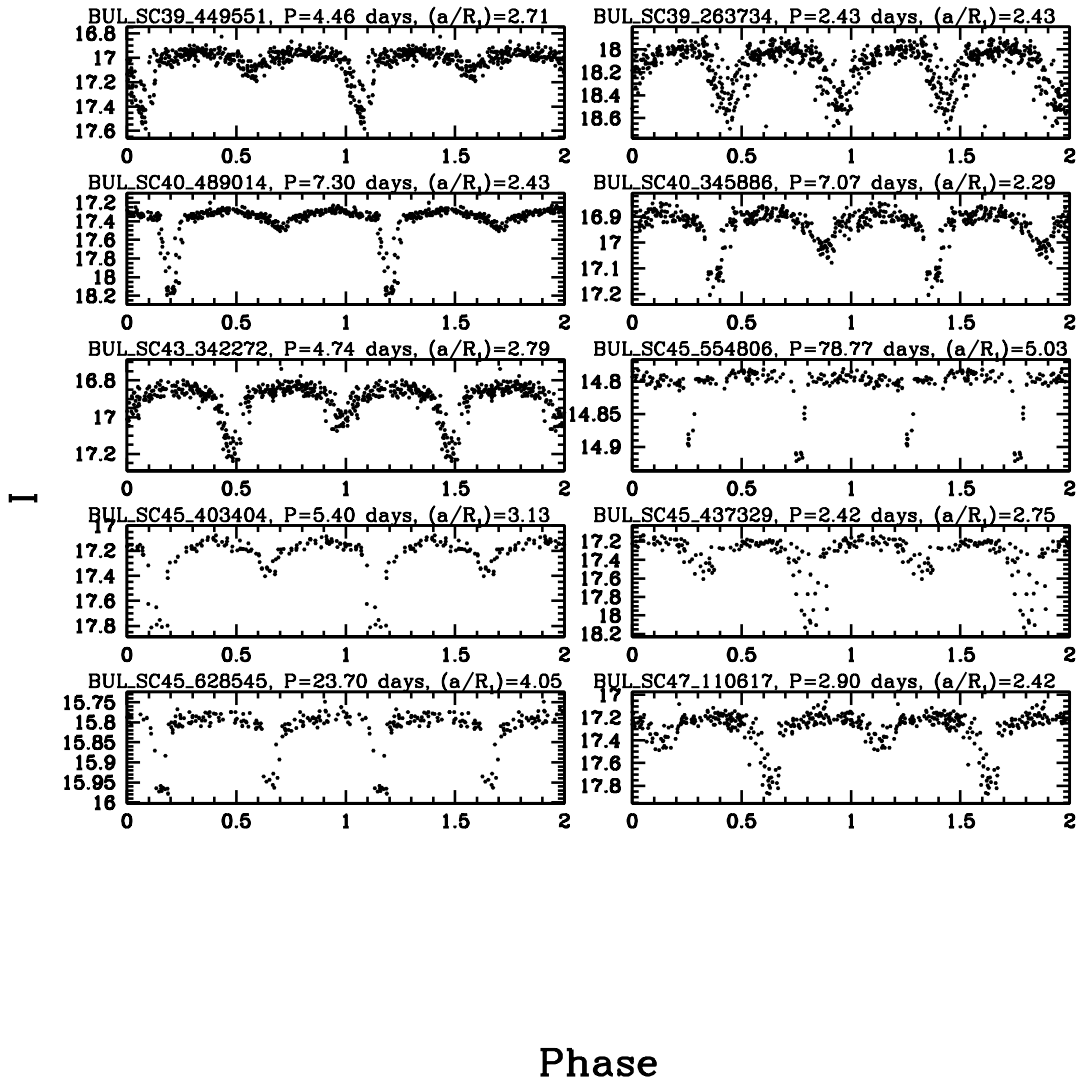


Figure 5: Same as in Fig. 3.

3. Stellar Models

We use the Yale Rotating Stellar Evolution Code (YREC, Delahaye *et al.* 2010) for the theoretical predictions provided in this work. The models are computed with diffusion. In order to match the observed atmospheric metals-to-hydrogen ratio $Z/X = 0.0229$ (Grevesse & Sauval 1998), solar radius R_{\odot} , and solar luminosity L_{\odot} at $t = 4.57$ Gyr, the models used in this work have the solar composition set to $(Z_{\odot}, Y_{\odot}) = (0.01875, 0.27357)$, and mixing length parameter α of 1.9449.

4. Early Scientific Payoffs of a Spectroscopic Survey of Detached Red Giant Eclipsing Binary Pairs

An early spin off of measurements of the Galactic Bulge detached RG eclipsing binary population would be either the validation or invalidation of several predictions derived from the age-helium-metallicity relations assumed and stated in the literature. The mass of RG stars is predicted to have the following functional dependence on metallicity, age and initial helium abundance:

$$\log(M/M_{\odot})_{p=-3.0} = 0.026 + 0.126[\text{M}/\text{H}] - 0.276\log(t/10) - 0.937(Y - 0.27), \quad (5)$$

and thus specific claims about the Bulge age-helium-metallicity relation derived from its CMD morphology predict equally specific mass-metallicity relations for Bulge RG stars. Fig. 6 shows that the mass-metallicity relations predicted are very distinct. For example, Bensby *et al.* (2011) assume isochrones with a standard helium-to-metals enrichment ratio and find that stars with $[\text{Fe}/\text{H}] = +0.35$ have an age of ~ 6 Gyr. If true, RGs at that metallicity should have masses of $\sim 1.35 M_{\odot}$. If this is the typical mass found for that metallicity it would confirm their interpretation, and would invalidate the hypothesis that the entire Bulge stellar population formed by rapid gravitational infall, an invalidation already suggested by dynamical investigations of metal-rich M-giants (Shen *et al.* 2010; Kunder *et al.* 2011). Alternatively, if the Bulge is enhanced in helium, as argued based on measurements of the Bulge red giant branch bump (RGBB) (Nataf *et al.* 2011a,b) and the discrepancy between spectroscopic and photometric turnoff ages (Nataf & Gould, 2011), then RG masses should be significantly lower. If $(\Delta Y/\Delta Z)_{\text{Bulge}} = 3$ and the population is older than $t = 10$ Gyr, no masses greater than $\sim 1 M_{\odot}$ should be measured on the RG branch.

The combination of RG mass and metallicity measurements with MSTO single-star spectroscopic measurements is enough to determine both the age-metallicity and helium-metallicity relationships of the bulge. Equation (??) shows that at fixed metallicity, increased age has the same effect as increased Y : both lead to decreased mass. This degeneracy has the opposite angle to that found on the MSTO and SGB: increased Y behaves similarly to *decreased* age, as both lead to higher temperatures on the MSTO and lower surface gravities on the SGB (Nataf & Gould 2011).

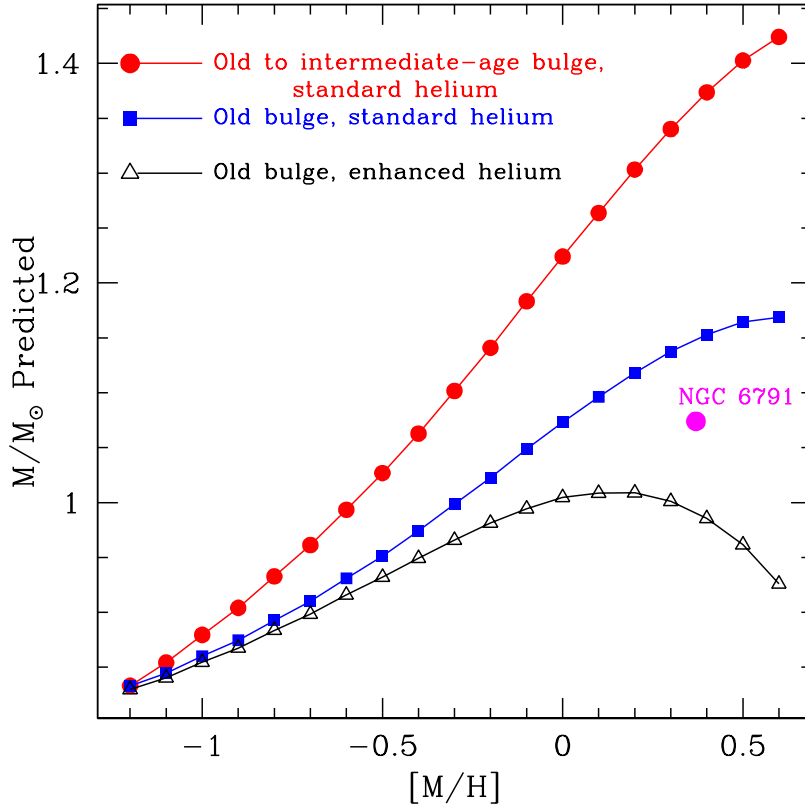


Figure 6: Different assessments of the age and helium abundance of the Bulge predict sharply distinct, easily-measurable RG mass-metallicity relationships. The old stellar population curves (blue,black) are characterized by age-metallicity relations that are linear with $\log(t/10)$ in the range $-1.2 \leq [M/H] \leq +0.6$, $10 \leq t/\text{Gyr} \leq 12$, whereas the old-to-intermediate age curve (red) assumes $5 \leq t/\text{Gyr} \leq 12$ over the same metallicity range. The enhanced-helium curve (black) assumes $\Delta Y/\Delta Z = 3$. We show the turnoff mass (expected to be a little smaller than the RG mass) for the old, metal-rich open cluster NGC 6791 (magenta), measured for an EB star by Grundahl *et al.* (2008)

There could also be a strong metallicity dependence to the binary fraction. Would the RG eclipsing binary metallicity-distribution function (MDF) match that of the measured Bulge RG MDF? If binaries are not a representative sample of the underlying population, a significant fraction of the Bulge stellar population might not be directly probe-able by this method. This would be interesting in its own right, as it could constrain models of how stars form in environments with different metallicity, an issue recently brought into sharper focus by Conroy & van Dokkum (2011). Moreover, there would still be value in measuring the age and helium abun-

dance of the Bulge within the remaining metallicity range.

These stars would also be powerful dynamical probes. As these are bright stars, their OGLE-III proper motions will be very precise. Their physical radii would measure where these stars are located in the Bulge relative to the RC. This would give the distance, and would enable conversion of proper motions into transverse velocities. The dynamics of the Bulge are known to be complex, with an X-shape at large separations ($Z \geq 500$ pc) from the plane recently discovered (Nataf *et al.* 2010; McWilliam & Zoccali 2010), and correlations between kinematics and metallicity at all latitudes (Babusiaux *et al.* 2010). A stellar sample with six measured kinematic phase space coordinates is needed.

Mass loss along the RG branch is another scientific prospect. Brown *et al.* (2011) found a significant number of low-mass white dwarfs without binary companions, implying that a significant number of stars skip stages of post-main-sequence stellar evolution, possibly due to enhanced mass loss in metal-rich stars. This would be consistent with the spectroscopic study of Rich *et al.* (2011), which showed that the $[\text{Fe}/\text{H}] \approx +0.35$ peak detected among Bulge dwarf and subgiant branch (SGB) stars (Bensby *et al.* 2010, 2011) is not present among Bulge M-giants. Significant mass loss would manifest itself as a much lower mass for more luminous stars, a characteristic that could easily be measured in a sufficiently large survey.

5. Population Parameters and Observables

The observable properties of a RG in an eclipsing binary pair are mass, density, metallicity, and effective temperature. These four observables can be matched to three theoretical quantities that effectively determine the initial state of the star (mass, helium, and metallicity), plus the evolutionary state at which we evaluate the stellar track. In principle, this match between the number of independent parameters and measurements enables complete determination of the age and helium abundance of each detached RG eclipsing binary pair. For the purposes of this section, we ignore theoretical uncertainties in the temperature and metallicity scale, and discuss what can be done if one assumes accurate stellar models and maximum-likelihood measurements and errors of the observables. We base our parametrization on $\log(\rho)$ rather than $\log g$ because the density, derived by plugging the EB lightcurve parameters into Kepler's 3rd law, is typically measured with substantially higher accuracy than the surface gravity.

Before moving forward, we must recognize that the accuracy of RG temperature estimates as well as the interpretive power thereof is a matter of ongoing controversy. There remains a ~ 100 K uncertainty in the temperature determination of stars (Casagrande *et al.* 2010), and this uncertainty is comparable in size to the predicted effects of large age or helium variations. Moreover, for the sample of close binaries listed in this work, $(R_{1,2}/a) \sim 0.2$, and thus star-star interactions may have a significant impact on the observed stellar properties (Chabrier *et al.*

2007). Additionally, the convective efficiency assumed in this work, parametrized by the mixing length, is calibrated on the sun, and there is no *a priori* reason why the efficiency should be the same in RGs. However, there remains value in working out the standard theoretical predictions, which may still be very effective for the most well-detached systems. The prospect of calibrating the zero-point terms for RG relationships are decent, due to the information accessible with missions such as *Kepler* (e.g. Hekker *et al.* 2010, 2011; Miglio *et al.* 2012). Additionally, whereas the interpretation of T_{eff} should be significantly impacted by these concerns, that of M/M_{\odot} should not – the mass observed in the RG phase is almost entirely a function of the main-sequence lifetime for a given initial mass, metallicity and helium abundance. Any EB with star-star interactions in the RG phase will not have experienced such interactions during the main-sequence, as $R_{1,2}/a$ will have been several times smaller.

Facilitating the task of parameter estimation is the fact that the observable properties are predicted to be linear or nearly linear in the parameter range of interest: stars of intermediate age and older. We use our library of stellar tracks to derive relationships for the parameter range $-3.5 \leq \log(\rho/\rho_{\odot}) \leq -2.5$, $-0.40 \leq [\text{M}/\text{H}] \leq 0.40$, $5 \leq t \leq 15$ Gyr, $0.25 \leq Y \leq 0.40$:

$$D_i = \kappa_{ij}\eta_j + D_{i0}, \quad (6)$$

where

$$D_i = \begin{pmatrix} Y \\ \log(t/10) \end{pmatrix}, \quad \eta_j = \begin{pmatrix} \log(T_{\text{eff}}) - 3.65 \\ [\text{M}/\text{H}] \\ \log(\rho/\rho_{\odot}) + 3 \\ \log(M/M_{\odot}) \end{pmatrix}, \quad (7)$$

and

$$\kappa_{ij} = \frac{\partial D_i}{\partial \eta_j} = \begin{pmatrix} 7.1208 & 0.28426 & -0.21878 & -0.50889 \\ -24.176 & -0.51046 & 0.7387 & -1.8901 \end{pmatrix}, \quad D_{i0} = \begin{pmatrix} 0.26516 \\ 0.10957 \end{pmatrix}. \quad (8)$$

The errors and covariance matrix in $D_i = (Y, \log(t/10))$ are given by

$$\sigma_i = \sqrt{C_{ii}}; \quad C_{ij} = \sum_{m,n=1}^4 \kappa_{im}\kappa_{jn}c_{mn} \quad (9)$$

where c_{ij} is the covariance matrix of the observables.

Equation (??) again emphasizes the crucial role of a mass measurement. Note that a change in any of the first three quantities ($\log T_{\text{eff}}$, $[\text{Fe}/\text{H}]$, $\log \rho$) induces motions of Y and $\log t$ in *opposite* directions, while a change in $\log M$ induces motion in the same direction. Therefore, without a tight mass measurement it is impossible to jointly constrain the helium content and age of the star. This is illustrated graphically in Fig. 7 and 8.

Fig. 7a shows the age-mass relation for RG stars at solar metallicity for different helium abundances. Note that the curves are both straight and equally spaced, i.e., a linear relation. This implies that perfect mass and metallicity measurements would yield a 1-dimensional linear constraint on the Y - $\log(t/10)$ plane. In fact, while an essentially perfect mass measurement is quite feasible (see below), this is not so for metallicity, as such the 1-dimensional constraint would be a band rather than a line.

This band is almost perfectly orthogonal to the constraint that can be obtained from spectroscopy ($\log T_{\text{eff}}$, $[\text{Fe}/\text{H}]$, $\log g$), which is shown in Fig. 8. Like the mass/metallicity constraint, spectroscopy by itself measures one fewer quantity than the number of model parameters being constrained, and thus is represented by parallel-line error contours, rather than closed contours. For purposes of this and subsequent plots, we begin with the covariance matrix $c_{ij} = e_i e_j \text{cor}_{ij}$, of a typical RG star (from Alves-Brito *et al.* 2010)

$$e_j = \begin{pmatrix} \sigma_{\log T_{\text{eff}}} \\ \sigma_{[\text{M}/\text{H}]} \\ \sigma_{\log g} \end{pmatrix} = \begin{pmatrix} 0.0044 \\ 0.161 \\ 0.184 \end{pmatrix}, \quad \text{cor}_{ij} = \begin{pmatrix} 1 & 0.36 & 0.39 \\ 0.36 & 1 & -0.64 \\ 0.39 & -0.64 & 1 \end{pmatrix}, \quad (10)$$

which has been derived directly from the ensemble of line measurements, using the method of Epstein *et al.* (2010). We then multiply the errors by a factor $2/3$, in recognition of the fact that the mass measurements will require multiple epochs of high S/N, high-resolution spectra.

We now turn to the impact of a ρ measurement, first combined only with spectroscopy (Eq. [??]) and then with a mass measurement as well. Unlike mass and metallicity, the other three quantities that one can hope to directly measure ($\log T_{\text{eff}}$, $\log \rho$, $\log g$) all depend strongly on phase of stellar evolution. In Fig. 7b,c, we show these tracks on the $\log T_{\text{eff}}/\log \rho$ plane for various values of Y and $\log(t)$ respectively. The main point to take away from these panels is that even if the age (panel b) or the helium content (panel c) were known exactly, it would be very difficult to distinguish the tracks from precise temperature and density measurements. Only if the mass is measured, so these two effects can be combined, do the tracks become well-separated (panel d).

The impact of a density measurement (combined with spectroscopy) on the age-helium plane is shown by the green curves in Fig. 8. Like the spectroscopy-only constraint (blue), these appear to be parallel lines, which is surprising given that there are four measurements ($\log T_{\text{eff}}$, $[\text{Fe}/\text{H}]$, $\log g$, $\log \rho$) to constrain four model parameters. In fact, these contours are part of an ellipse which is extremely elongated in the direction orthogonal to the mass constraint. The reason for this is essentially the same as spectroscopy-only case: weak coupling of $\log M$ to Y and $\log t$ via error propagation from the $\log g$ measurement. Fig. 8 also shows the impact of adding a mass measurement to either of these cases. When all measurements are combined, the error ellipse is highly elongated along the direction of the

mass-constraint, with its width essentially determined by the metallicity error. Note the $\log M$ and $\log \rho$ measurements have both been assumed to have errors of 0.01 dex (2.3%). However, this diagram would look almost exactly the same if we had assumed zero errors for both quantities. Hence, even conservative error bars are equivalent to perfect measurements for the $\log M$ and $\log \rho$. We note that the detached RG EB twins OGLE SC10 137844, whose parameters are somewhat more difficult to measure due to the fact they are in a highly eccentric ($e = 0.31$) and long-period system ($P = 372$ days), recently had their masses measured to $\sim 0.8\%$ and densities to $\sim 4.5\%$ (Graczyk *et al.* 2012).

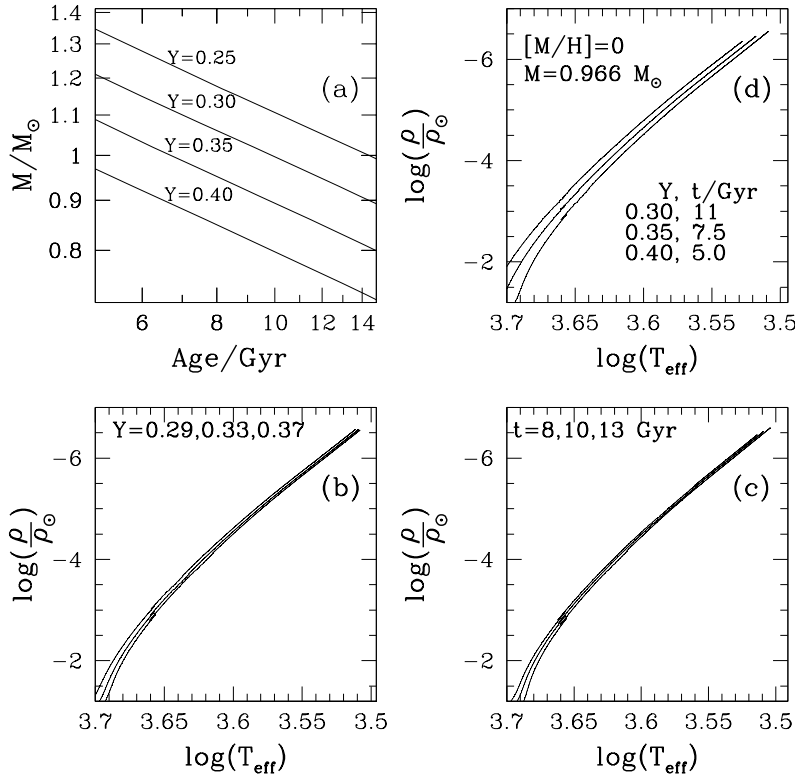


Figure 7: Predicted relationships between RG parameters and observables. Panel (a) M/M_{\odot} as a function of age for $[M/H]=0$ tracks varying in initial helium. Lower mass means higher age or higher helium. Panel (b) RG tracks with $[M/H]=0$, $t = 11$ Gyr varying in initial helium. Higher helium at fixed metallicity and density implies a hotter RG branch. Panel (c) RG tracks with solar chemistry varying in age. Higher age at fixed chemistry and density implies a colder RG branch. Panel (d) These two effects add constructively when the mass is fixed, because age goes down as helium abundance goes up.

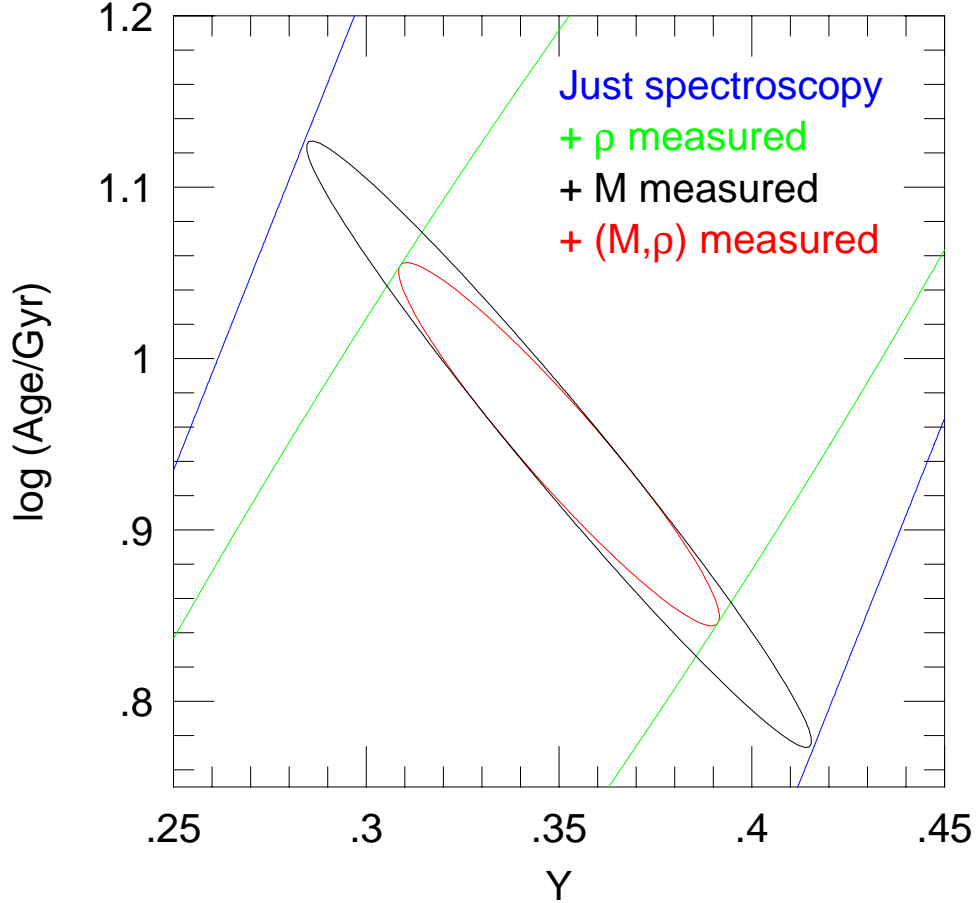


Figure 8: Predicted constraints on the age-helium plane from spectroscopy only ($\log T_{\text{eff}}, [\text{Fe}/\text{H}], \log g$) (blue), spectroscopy plus density measurement (green), spectroscopy plus mass measurement (black), and all measurements (red), assuming measured properties ($M/M_{\odot}, [\text{M}/\text{H}], T_{\text{eff}}, \log(\rho/\rho_{\odot}) + 3$) = $(0.91 \pm 0.01, 0.0 \pm 0.1, 4563 \pm 30, 0 \pm 0.01)$. With just spectroscopy, age and helium are completely degenerate. Even precise measurement of the density only narrows this degeneracy, it does not effectively break it. On the other hand, a mass measurement generates an orthogonal constraint on this plane and so does, by itself, break the degeneracy. Combining mass and density measurements then further reduces the errors by a factor 1.6.

The actual spectroscopic measurements would be greatly constrained by the eclipsing binary lightcurve. Aside from the precisely measured values of $\log g$ obtained from $\log \rho$ and M/M_{\odot} , relative temperatures and luminosities would be known to a high degree of accuracy from the photometry alone, reducing the degrees of freedom allowed in the spectroscopic fit. That the two stars are in a moderately close binary would strongly suggest that they have identical metallicities. Further, the ability to take spectra during eclipse, when only the larger and thus brighter star would contribute to the spectrum, guarantees spectroscopic parameters at least as good as those of a single RG. We note that for these systems the eclipses often last several days, making the acquisition of single-star spectra very feasible. We also comment on an important recent finding. Gonzalez *et al.* (2011) used dereddened near-IR photometry of the Galactic Bulge and showed that the photometric color distribution of Bulge stars was in itself sufficient to reproduce the spectroscopic Bulge metallicity distribution function. This demonstrates that the Bulge RG temperatures are well-behaved.

6. Discussion

6.1. *The Effect of Uncertainties in Stellar Evolution Models*

The stellar models that are used to interpret the measurements are themselves a source of uncertainty. Heavy element diffusion, the value of the mixing length, and angular momentum evolution are among the uncertainties of stellar evolution. Whereas mass and metallicity measurements should yield immediate and powerful constraining power, temperature measurements will be more difficult to interpret due to their greater theoretical uncertainties. This is due to the fact that stellar models are typically calibrated with respect to the Sun, a main-sequence star. Thus main-sequence behavior (e.g., main-sequence lifetime as a function of mass and composition) is better calibrated than post-main-sequence behavior. Interpreting RG temperatures will therefore require greater care than interpreting masses. There will be at least three different means to constrain the impact of these uncertainties.

We ran several models with varied input parameters to gauge the effect of two of the most significant uncertainties: the mixing length and diffusion. Reducing the mixing length to 1.6449 from 1.9449, a shift comparable in size to the empirical (Ferraro *et al.* 2006) and theoretical (Trampedach & Stein 2011) determinations of the uncertainty, has the effect of increasing the stellar lifetime at fixed mass, metallicity and helium by $\sim 1\%$ – the effect is negligible. For diffusion, we computed the same models *without* diffusion, an exaggeration of the size of the error in diffusion, and these yielded a stellar lifetime decrease of $\sim 3\%$. Note that turning off diffusion requires small changes in the metals abundance and the mixing length to maintain consistency with the solar constraints, see Table 1 of van Saders & Pinsonneault (2012). Both effects are smaller than the statistical error resulting from a typical precision in the metallicity of ~ 0.1 dex. We also verified that the mass

predictions for RG stars in this work agree with those of the BaSTI (Pietrinferni *et al.* 2006) and Dartmouth (Dotter *et al.* 2008) stellar databases – agreement is to $\sim 1\%$ on the lower RGB.

An excellent way to constrain the effect of theoretical uncertainties would be to exploit the fact that the relative predictions of stellar evolution models are more reliable than the absolute predictions. A reasonable choice for an anchor point would be requiring the most metal-poor stars to have the same age as the Galactic globular clusters, $t_{GC} = 12.8 \pm 0.4$ Gyr (Marín-Franch *et al.* 2009), and to have a primordial helium abundance for those stars of $Y = 0.249$ (Simha & Steigman 2008). In principle, the metal-poor Bulge may in fact be a little older: Bulge RR Lyrae stars are more metal-rich than those in globular clusters (Kunder & Chaboyer 2008; Pietrukowicz *et al.* 2011), which might imply that the most metal-poor Bulge stars are too old to generate many RR Lyrae stars. However, since the age difference between the GCs and the universe is not large, such a difference would not significantly undermine the use of the GCs as an age anchor point.

At Disk-like metallicities (i.e. $[\text{Fe}/\text{H}] \sim -0.3$), there is a campaign to measure precise abundances of RG stars that have asteroseismic measurements from the *Kepler* and *CoRoT* satellites (Epstein *et al.*, NOAO-2011A-0510). Due to the fact that these are Disk stars, which are expected to have younger ages and likely different helium-enrichment patterns, we should expect that the $\log g - T_{\text{eff}} - [\text{M}/\text{H}]$ mapping will not be identical to the mapping that can be obtained for Bulge stars. It will be interesting to see how they differ. The differences would be combined with the predictions of Equation (??) to yield estimates of the relative age and helium offsets between these two stellar populations.

At the metal-rich end, the open cluster NGC 6791 is a potent anchor. It has a high metallicity $[\text{Fe}/\text{H}] = +0.40$, it is the subject of detailed asteroseismic study from *Kepler* photometry (Miglio *et al.* 2012), and has a main-sequence-turnoff eclipsing binary with measured masses and radii (Grundahl *et al.* 2008). An interesting finding of Miglio *et al.* (2012) is that the mass-loss for the metal-rich RG stars in NGC 6791 is not large: $\Delta \bar{M} = (0.19 \pm 0.04) M_{\odot}$. However, this finding is suggestive rather than conclusive due to the use of first-order asteroseismic scaling relations, which are still a matter of ongoing investigation. A direct mass measurement of mass-loss would be helpful, and this could be detected if it were found that RG stars at the same metallicity have a luminosity-dependent mass. With enough luck, one or several EBs at large periods may even be found on the RC phase of stellar evolution. Short-period EBs with RC members would not be adequate, as it is likely that these detached EBs would not have been detached when the RC was a much larger upper-RG branch star.

The combined use of these three anchors and the relative predictions of stellar evolution could overdetermine the properties of Bulge stars. Because they span the entire metallicity range $-1.2 \leq [\text{M}/\text{H}] \leq +0.60$ (Zoccali *et al.* 2008; Johnson *et al.* 2011; Hill *et al.* 2011), any residual uncertainty could be used to place bounds

on the uncertainties in stellar models.

6.2. Other Uncertainties

There are several systematic effects that could pose challenges to any survey of eclipsing binary pairs. We show, however, that these could either be controlled or become investigative avenues in their own right.

The first is that blending can affect the lightcurve of Bulge eclipsing binaries, a systematic that is not generally a concern in the solar neighborhood. The extra flux from a blend, F_b , would bias the interpretation of the flux drop during the eclipse, and thus the value of the derived stellar density. In our appendix, we derive that:

$$\Delta \ln(\rho_1) = -\frac{3 F_b}{4 F_1}. \quad (11)$$

It follows from Equations (??) and (??) that a 10% blend would significantly affect the derived stellar parameter values. This could be controlled by getting high-resolution images of the target in *JHK*. A significant blend could also be estimated from its contribution to the spectra, as its spectral lines would not share the $\sim 100 \text{ km s}^{-1}$ orbital velocities. Thus, it is likely that the blending fraction F_b/F_1 could be measured to a precision of a few percent.

The second effect is the RGBB. This post-main-sequence phase of stellar evolution, during which the star temporarily gets fainter, before getting brighter again (Cassisi & Salaris 1997; Bjork & Chaboyer 2006; Nataf *et al.* 2011b), breaks the injective mapping between density and temperature at fixed mass, helium and metallicity. The resulting difference in temperature can yield an offset in the derived values of $\delta Y \sim 0.007$ and $\delta \log(t/10) \sim 0.02$. However, this would only occur at the position of the RGBB, which can be easily estimated to a precision of ~ 0.04 dex in $\log g$ (i.e. ~ 0.1 mag) as its characteristic luminosity and number counts are steep, empirically-calibrated functions of metallicity (Nataf *et al.* 2011b). The lifetime of the RGBB for Bulge stars (~ 20 Myr, Nataf *et al.* 2011a) does not contribute to the total age uncertainty, as independent errors add in quadrature, and that of the metallicity determination would dominate.

The third issue is that of RS Canum Venaticorum (RS CVn) type stars (Eaton & Hall 1979). These heavily spotted systems, common in binaries, would have effective temperatures distinct from those predicted by naive models. If close-in binaries were found to have lower temperatures at fixed density and metallicity, this would demonstrate an effect due to tides and angular momentum transfer. The superior photometry from OGLE-III, with its greater cadence, longer baseline, and higher precision, should impose upper bounds on the spot depth of eclipsing binary candidates, which could be further investigated by measuring the calcium H+K emission in the spectra. We note that identification of RS CVn could be a good way to identify binaries that are not RG-EB twins, which would be a means of expanding the sample.

Stellar rotation could also be a concern. While isolated solar-mass stars tend to spin down over time, their cousins in binary systems are tidally circularized after 7 Gyr for periods $P < 15$ days and after 12 Gyr for periods $P < 20$ days (Mathieu *et al.* 2004). Although tidal synchronization is not the same as circularization, the two are closely related. Thus, at least the closer RG eclipsing systems were probably rotating faster than the Sun ($P = 25$ day) while they were on the main sequence. Sills *et al.* (2000) showed that at fixed mass and composition, RG stars whose progenitors were rotating with periods $P = 8$ day are predicted to be slightly colder than non-rotating RG stars yielding an estimated systematic effect of $\Delta Y \sim 0.01$. Since the RG eclipsing binaries are at longer periods, the effect will be even smaller, but should nevertheless be taken into account.

7. Conclusion

We have demonstrated that there are observable, detached RG eclipsing binary pairs in the Galactic Bulge, and have constructed gold and silver samples of 34 and 248 candidates respectively by imposing strict physical consistency requirements on the total OGLE-II eclipsing binary sample of Devor (2005). We have demonstrated that the derived masses, temperatures, metallicities and densities assuming reasonable error estimates would give powerful constraints on the formation and evolution of the Galaxy: both the age and helium abundance would be tightly constrained, at every measured metallicity. In addition to providing fundamental insights on Milky Way assembly, a survey of these systems would have the potential to teach us about the metallicity-dependence of the binary fraction, mass loss on the RG branch and stellar models. Our count of 34-(282) such systems in the OGLE-II eclipsing binary catalog leads us to estimate that at least 200-(1500) could be found in OGLE-III, just from the larger viewing area.

Acknowledgements. DMN was primarily supported by the NSERC grant PGSD3-403304-2011. DMN and AG were partially supported by the NSF grant AST-1103471. MHP was partially supported by NASA grant NNX11AE04G. We thank Jan Skowron, Jason Eastman, Frank Fekel and Martin Asplund for helpful discussions.

REFERENCES

- Al-Naimiy, H. M. 1978, *Astrophysics and Space Science*, **53**, 181.
 Alves-Brito, A., Meléndez, J., Asplund, M., Ramírez, I., & Yong, D. 2010, *A&AS*, **513**, A35.
 Assef, R. J., Gould, A., Afonso, C., *et al.* 2006, *ApJ*, **649**, 954.
 Babusiaux, C., Gómez, A., Hill, V., *et al.* 2010, *A&AS*, **519**, A77.
 Bensby, T., Feltzing, S., Johnson, J. A., *et al.* 2010, *A&AS*, **512**, A41.
 Bensby, T., Adén, D., Meléndez, J., *et al.* 2011, *A&AS*, **533**, A134.
 Bessell, M. S., & Brett, J. M. 1988, *PASP*, **100**, 1134.
 Bjork, S. R., & Chaboyer, B. 2006, *ApJ*, **641**, 1102.

- Brown, J. M., Kilic, M., Brown, W. R., & Kenyon, S. J. 2011, *ApJ*, **730**, 67.
- Casagrande, L., Ramírez, I., Meléndez, J., Bessell, M., & Asplund, M. 2010, *A&AS*, **512**, A54.
- Cassisi, S., & Salaris, M. 1997, *MNRAS*, **285**, 593.
- Chabrier, G., Gallardo, J., & Baraffe, I. 2007, *A&AS*, **472**, L17.
- Clarkson, W. I., Sahu, K. C., Anderson, J., *et al.* 2011, *ApJ*, **735**, 37.
- Collinge, M. J., Sumi, T., & Fabrycky, D. 2006, *ApJ*, **651**, 197.
- Conroy, C., & van Dokkum, P. 2011, *arXiv:1109.0007*.
- Delahaye, F., Pinsonneault, M. H., Pinsonneault, L., & Zeppen, C. J. 2010, *arXiv:1005.0423*.
- Devor, J. 2005, *ApJ*, **628**, 411.
- Dotter, A., Chaboyer, B., Jevremović, D., *et al.* 2008, *ApJS*, **178**, 89.
- Duquenooy, A., & Mayor, M. 1991, *A&AS*, **248**, 485.
- Eaton, J. A., & Hall, D. S. 1979, *ApJ*, **227**, 907.
- Epstein, C. R., Johnson, J. A., Dong, S., *et al.* 2010, *ApJ*, **709**, 447.
- Epstein, C. R., Johnson, J. A., Pinsonneault, M.H., Lai, David 2010, *NOAO-2011A-0510*.
- Ferraro, F. R., Valenti, E., Straniero, O., & Origlia, L. 2006, *ApJ*, **642**, 225.
- Fulbright, J. P., McWilliam, A., & Rich, R. M. 2006, *ApJ*, **636**, 821.
- Gonzalez, O. A., Rejkuba, M., Zoccali, M., *et al.* 2011, *A&AS*, **530**, A54.
- Gonzalez, O. A., Rejkuba, M., Zoccali, M., Valenti, E., & Minniti, D. 2011, *A&AS*, **534**, A3.
- Graczyk, D., Pietrzynski, G., Thompson, I. B., *et al.* 2012, *arXiv:1203.2517*.
- Grevesse, N., & Sauval, A. J. 1998, *Space Science Reviews*, **85**, 161.
- Grundahl, F., Clausen, J. V., Hardis, S., & Frandsen, S. 2008, *A&AS*, **492**, 171.
- Hekker, S., Debosscher, J., Huber, D., *et al.* 2010, *The Astrophysical Journal Letters*, **713**, L187.
- Hekker, S., Gilliland, R. L., Elsworth, Y., *et al.* 2011, *MNRAS*, **414**, 2594.
- Hill, V., Lecureur, A., Gómez, A., *et al.* 2011, *A&AS*, **534**, A80.
- Johnson, C. I., Rich, R. M., Fulbright, J. P., Valenti, E., & McWilliam, A. 2011, *ApJ*, **732**, 108.
- Kervella, P., Thévenin, F., Di Folco, E., & Ségransan, D. 2004, *A&AS*, **426**, 297.
- Kuiper, G. P. 1935, *PASP*, **47**, 15.
- Kunder, A., & Chaboyer, B. 2008, *AJ*, **136**, 2441.
- Kunder, A., Koch, A., Rich, R. M., *et al.* 2011, *arXiv:1112.1955*.
- Lucy, L. B. 1967, *Zeitschrift für Astrophysik*, **65**, 89.
- Marín-Franch, A., Aparicio, A., Piotto, G., *et al.* 2009, *ApJ*, **694**, 1498.
- Martins, F., Gillessen, S., Eisenhauer, F., *et al.* 2008, *The Astrophysical Journal Letters*, **672**, L119.
- Mathieu, R.D., Meibom, S., & Dolan, C.J. 2004, *ApJ*, **682**, L121.
- McWilliam, A., & Zoccali, M. 2010, *ApJ*, **724**, 1491.
- Miglio, A., Brogaard, K., Stello, D., *et al.* 2012, *MNRAS*, **419**, 2077.
- Morris, S. L. 1985, *ApJ*, **295**, 143.
- Nataf, D. M., Stanek, K. Z., & Bakos, G. A. 2009, *Acta Astron.*, **59**, 255.
- Nataf, D. M., Udalski, A., Gould, A., Fouqué, P., & Stanek, K. Z. 2010, *The Astrophysical Journal Letters*, **721**, L28.
- Nataf, D. M., Stanek, K. Z., & Bakos, G. A. 2010, *Acta Astron.*, **60**, 261.
- Nataf, D. M., Udalski, A., Gould, A., & Pinsonneault, M. H. 2011, *ApJ*, **730**, 118.
- Nataf, D. M., Gould, A. P., Pinsonneault, M. H., & Udalski, A. 2011, *arXiv:1109.2118*.
- Nataf, D. M., & Gould, A. P. 2011, *arXiv:1112.1072*.
- Pasquini, L., Mauas, P., Käufel, H. U., & Cacciari, C. 2011, *A&AS*, **531**, A35.
- Pietrinferni, A., Cassisi, S., Salaris, M., & Castelli, F. 2004, *ApJ*, **612**, 168.
- Pietrukowicz, P., Udalski, A., Soszynski, I., *et al.* 2011, *arXiv:1107.3152*.
- Pinsonneault, M. H., & Stanek, K. Z. 2006, *The Astrophysical Journal Letters*, **639**, L67.
- Pribulla, T., & Rucinski, S. M. 2006, *AJ*, **131**, 2986.
- Renzini, A., & Buzzoni, A. 1986, *Spectral Evolution of Galaxies*, **122**, 195.
- Rich, R. M., Origlia, L., & Valenti, E. 2011, *arXiv:1112.0306*.
- Salpeter, E. E. 1955, *ApJ*, **121**, 161.
- Shen, J., Rich, R. M., Kormendy, J., *et al.* 2010, *The Astrophysical Journal Letters*, **720**, L72.

- Sills, A., Pinsonneault, M. H., & Terndrup, D. M. 2000, *ApJ*, **534**, 335.
 Simha, V., & Steigman, G. 2008, *Journal of Cosmology and Astroparticle Physics*, **8**, 11.
 Soszyński, I., Dziembowski, W. A., Udalski, A., *et al.* 2011, *Acta Astron.*, **61**, 1.
 Szymanski, M. K. 2005, *Acta Astron.*, **55**, 43.
 Szymański, M. K., Udalski, A., Soszyński, I., *et al.* 2011, *Acta Astron.*, **61**, 83.
 Tokovinin, A., Thomas, S., Sterzik, M., & Udry, S. 2006, *A&AS*, **450**, 681.
 Trampedach, R., & Stein, R. F. 2011, *ApJ*, **731**, 78.
 Udalski, A., Kubiak, M., & Szymanski, M. 1997, *Acta Astron.*, **47**, 319.
 van Saders, J. L., & Pinsonneault, M. H. 2012, *ApJ*, **746**, 16.
 Zoccali, M., Hill, V., Lecureur, A., *et al.* 2008, *A&AS*, **486**, 177.

Appendix: Effect of Blending on Derived Eclipsing Binary Parameters

In this Appendix, we derive the error made in estimating the densities of the binary components made by failing to detect (and so take into account) blending by a third star within the PSF. For this purpose, we make the simplifying assumptions of uniform surface brightness and highly unequal source sizes. If these assumptions are relaxed, the derivation becomes much more complicated, but the final results are similar.

Define

$$\tau_1 \equiv \pi \frac{t_1}{P} \quad \tau_2 \equiv \pi \frac{t_2}{P} \quad z_1 \equiv \frac{r_1}{a}; \quad z_2 \equiv \frac{r_2}{a}$$

where t_1 is the transit time, t_2 is the ingress time, P is the period, a is the semimajor axis, and r_1 and r_2 are the two radii. Note that t_i and P can be measured with essentially infinite precision, because they depend only on timing data, and not on blending. Hence, τ_i are also observables with quasi-infinite precision. Then, for circular orbits,

$$\tau_1 = z_1(1 - \beta^2)^{1/2} \quad \tau_2 = z_2(1 - \beta^2)^{-1/2}$$

where β is the impact parameter. Hence, the precision of

$$\beta = \sqrt{1 - \frac{\tau_1 z_2}{\tau_2 z_1}} = \sqrt{1 - \frac{t_1 r_2}{t_2 r_1}} \quad z_1 z_2 = \tau_1 \tau_2$$

depends directly on how well the ratio of radii, r_2/r_1 can be measured.

The fluxes in and out of eclipse are related to the two surface brightnesses by

$$F_1 = \pi S_1 r_1^2; \quad F_2 = \pi[S_1(r_1^2 - r_2^2) + S_2 r_2^2] = F_1 + \pi(S_2 - S_1)r_2^2 \quad F_3 = F_1 + \pi S_2 r_2^2$$

Hence,

$$\frac{F_2 - F_1}{F_3 - F_1} = 1 - \frac{S_1}{S_2}; \Rightarrow \frac{S_1}{S_2} = \frac{F_3 - F_2}{F_3 - F_1}$$

$$\frac{F_3 - F_1}{F_1} = \frac{S_2}{S_1} \frac{r_2^2}{r_1^2} \Rightarrow \frac{r_2^2}{r_1^2} = \frac{F_3 - F_2}{F_1} \Rightarrow \eta \equiv \frac{z_2}{z_1} = \frac{r_2}{r_1} = \sqrt{\frac{F_3 - F_2}{F_1}},$$

where $\eta \equiv z_2/z_1$. The inverse density of the whole system is given

$$\frac{1}{\rho} = \frac{4\pi r_1^3 + r_2^3}{3M} = \frac{4\pi a^3}{3M} (z_1^3 + z_2^3) = \frac{G}{3\pi} P^2 (z_1^3 + z_2^3) = \frac{G}{3\pi} P^2 z_1^3 (1 + \eta^3)$$

$$z_1 = \sqrt{\frac{\tau_1 \tau_2}{\eta}} \Rightarrow$$

$$\frac{1}{\rho} = \frac{G}{3\pi} P^2 (\tau_1 \tau_2)^{3/2} (\eta^{3/2} + \eta^{-3/2}) = \frac{\pi^2 G (t_1 t_2)^{3/2}}{3P} (\eta^{-3/2} + \eta^{3/2})$$

And, if the two masses are known (or assumed) to be equal:

$$\frac{1}{\rho_1} = \frac{2\pi^2 G (t_1 t_2)^{3/2}}{3P} \eta^{3/2} = \frac{2\pi^2 G (t_1 t_2)^{3/2}}{3P} \left(\frac{F_1}{F_3 - F_2} \right)^{3/4}$$

Now, the hardest thing to measure (assuming no blending) will be t_2 (ingress time). This is relatively short, so few data points. Plus, one must actually understand limb darkening quite well to measure it. The only quantity susceptible to blending is η . If the system is blended by flux F_b , then all three fluxes F_1, F_3, F_3 are increased by this same amount. In this case,

$$\frac{d \ln \eta^2}{d F_b} = -\frac{1}{F_1} \Rightarrow \frac{d \ln \rho_1}{d F_b} = -\frac{3}{4} \frac{1}{F_1} \Rightarrow \Delta \ln \rho_1 = -\frac{3}{4} \frac{F_b}{F_1}$$

Blending can be controlled in two complementary ways. First, high-resolution images on 8m class telescopes should be able to detect all sources within 2 FWHM of the target, down to 1–2% in *JHK*. Translating these fluxes into *I*-band will involve some error, but should be statistically unbiased.

Second, any ambient source within the optical PSF with 1–2% of target flux can be detected as follows. Since the periods are typically $P = 20$ days, the two sources will have relatively motion roughly 100 km s^{-1} , while the line-widths should be smaller by a factor $r/2a$, even if the stars are tidally locked. Therefore, the line systems of the two stars should be quite well separated, enabling excellent empirical templates of both from the ensemble of RV spectra. Then these templates can be subtracted from each spectrum, shifted by the fit velocity. The sum of the residuals of these fits will give a S/N \sim few spectrum of any ambient light, certainly enough to identify its source.

Table 1: We tabulate the OGLE-II identification, coordinates, apparent magnitudes, relative radii and periods for the gold (top) and silver (bottom) sample RG eclipsing binary pairs identified. More detailed properties can be found in the catalog of Devor (2005) from which these candidates were identified. E_1 is the epoch of the eclipse when the secondary is behind the primary. The star IDs used here are those from Devor (2005). The original photometry for these sources can be found on the OGLE-II archive (Udalski *et al.* 1997; Szymanski *et al.* 2005).

Field	ID	RA	DEC	$(V - I)$	I	R_1/a	R_2/a	period (days)
3	2325	17:53:15.31	-30:07:57.2	2.398	16.977	0.375	0.263	4.488256
3	2823	17:53:55.27	-30:05:18.9	2.133	17.214	0.329	0.249	3.930081
3	2929	17:53:45.96	-30:04:33.6	2.245	17.604	0.370	0.276	3.471413
3	7715	17:53:31.11	-29:34:38.7	2.417	16.969	0.345	0.222	5.883186
4	830	17:54:33.33	-30:06:18.3	2.477	16.781	0.392	0.305	7.477364
4	831	17:54:35.36	-30:06:23.2	2.326	17.744	0.392	0.346	2.403032
4	1290	17:55:01.80	-30:03:44.6	2.388	17.356	0.346	0.268	4.055058
5	1889	17:50:35.23	-30:09:19.5	3.664	18.061	0.362	0.279	7.024886
7	1089	18:08:53.56	-31:54:48.1	1.362	16.659	0.310	0.280	3.112654
9	132	18:24:17.25	-22:10:52.1	1.989	16.577	0.414	0.276	3.336563
9	1502	18:24:07.57	-21:31:22.4	1.787	16.390	0.384	0.306	3.458615
13	1282	18:17:07.41	-24:03:03.3	2.112	16.314	0.255	0.105	12.277672
14	3912	17:47:11.83	-22:42:21.1	2.288	17.316	0.403	0.269	4.758608
24	1374	17:53:38.18	-33:01:25.4	2.193	17.368	0.426	0.248	4.623804
24	2461	17:53:03.90	-32:45:12.4	2.423	16.021	0.329	0.190	21.687112
30	1600	18:01:22.55	-29:03:24.0	1.929	17.316	0.278	0.233	4.671058
30	6658	18:01:27.97	-28:24:07.8	1.946	15.935	0.354	0.272	9.952315
31	631	18:02:14.25	-28:56:11.2	1.945	16.331	0.370	0.289	3.937200
31	2641	18:02:10.51	-28:30:10.2	1.768	16.657	0.307	0.222	5.033917
34	1369	17:58:11.35	-29:24:54.4	2.610	17.027	0.410	0.251	6.113610
34	6500	17:57:57.95	-28:48:09.3	2.045	17.238	0.360	0.261	3.436820
37	1846	17:52:30.15	-30:11:44.6	2.331	17.367	0.344	0.311	2.934912
37	6396	17:52:35.36	-29:40:28.6	2.619	16.767	0.294	0.190	7.772554
37	7093	17:52:15.51	-29:36:14.2	3.147	17.517	0.254	0.232	6.784166
39	1159	17:55:53.47	-30:02:53.9	2.385	17.154	0.369	0.217	4.455969
39	1604	17:55:31.28	-29:59:03.9	2.574	18.199	0.411	0.320	2.430296
40	310	17:51:33.38	-33:39:04.9	2.682	17.419	0.412	0.294	7.297005
40	621	17:51:18.82	-33:33:59.8	2.459	17.004	0.436	0.204	7.069012
43	3095	17:35:17.21	-26:47:27.8	2.439	16.954	0.359	0.279	4.740494
45	1064	18:04:04.03	-30:03:52.2	2.048	14.894	0.199	0.058	78.765788
45	1155	18:03:44.62	-30:01:55.3	1.956	17.143	0.319	0.243	5.400987
45	1522	18:03:42.13	-29:53:05.3	1.640	17.350	0.364	0.358	2.424248

45	2170	18:03:57.10	-29:39:36.7	2.122	15.881	0.247	0.090	23.699590
47	481	17:27:01.35	-39:50:21.5	1.778	17.383	0.413	0.315	2.898527
1	1713	18:02:46.29	-30:04:30.5	2.154	16.330	0.140	0.076	5.663370
1	2513	18:02:08.29	-29:53:53.5	1.916	15.160	0.426	0.265	2.359235
1	2938	18:02:02.94	-29:48:30.5	1.662	16.311	0.375	0.164	2.903954
1	3738	18:03:01.96	-29:40:20.3	1.710	17.608	0.267	0.264	3.551679
1	3846	18:02:42.99	-29:38:47.2	1.818	16.510	0.289	0.097	7.779557
1	3859	18:02:49.68	-29:38:41.0	1.889	17.665	0.391	0.191	2.949637
2	892	18:04:35.40	-29:11:58.1	1.764	16.882	0.416	0.145	4.541277
2	1301	18:04:24.76	-29:07:16.1	1.628	16.505	0.253	0.079	6.464870
2	1800	18:04:09.41	-29:00:56.9	1.506	17.095	0.300	0.199	2.339578
2	2542	18:04:54.38	-28:53:55.9	1.395	15.973	0.360	0.208	3.085778
2	3673	18:04:45.22	-28:42:13.0	1.673	17.379	0.322	0.088	12.985678
2	3894	18:04:19.55	-28:39:46.3	1.597	17.256	0.338	0.164	3.335057
2	4754	18:04:10.21	-28:30:05.0	1.662	17.289	0.325	0.203	2.130568
3	1149	17:53:11.82	-30:16:45.6	2.844	16.814	0.421	0.187	3.295681
3	1688	17:53:58.88	-30:13:45.6	2.052	17.444	0.381	0.214	2.479170
3	2195	17:53:15.24	-30:08:44.6	2.224	16.433	0.418	0.159	3.179790
3	3488	17:53:53.48	-30:01:21.8	2.328	18.132	0.259	0.204	2.156910
3	3489	17:53:54.82	-30:00:46.7	2.652	16.082	0.283	0.082	2.943854
3	3547	17:53:25.67	-30:00:01.5	2.635	17.816	0.266	0.228	2.474109
3	3744	17:54:04.47	-29:59:15.8	2.335	17.619	0.335	0.272	3.511041
3	6413	17:53:31.09	-29:41:39.3	2.382	16.943	0.322	0.182	8.528036
3	8222	17:53:55.24	-29:31:35.3	2.469	17.493	0.297	0.242	7.623718
3	8395	17:53:16.26	-29:30:30.0	3.095	17.369	0.418	0.257	5.337132
4	1047	17:54:10.50	-30:04:31.6	2.063	16.928	0.316	0.176	2.075691
4	1120	17:54:44.27	-30:04:11.8	2.206	16.953	0.448	0.227	7.343176
4	1224	17:54:21.76	-30:03:07.7	2.226	17.284	0.362	0.216	5.331105
4	1289	17:54:57.96	-30:03:31.4	2.317	18.168	0.267	0.200	3.543221
4	3707	17:54:58.48	-29:49:18.1	1.824	17.100	0.300	0.198	2.381842
4	4049	17:54:41.33	-29:47:16.7	2.424	16.459	0.119	0.103	3.842130
4	4449	17:54:07.59	-29:44:58.6	2.321	15.552	0.572	0.129	2.269646
4	4564	17:54:57.61	-29:45:02.3	2.502	17.463	0.328	0.211	3.350001
4	5392	17:54:17.17	-29:39:20.2	2.294	16.289	0.162	0.105	2.820490
4	6839	17:54:39.93	-29:30:30.7	2.033	17.402	0.319	0.227	2.379704
4	6905	17:54:18.89	-29:29:39.7	2.137	18.454	0.305	0.296	3.514754
4	7346	17:54:12.23	-29:27:05.6	2.371	17.937	0.323	0.247	2.697201
4	8604	17:54:10.56	-29:18:18.2	2.488	18.280	0.201	0.128	4.274822
5	5124	17:49:58.22	-29:44:04.5	4.193	17.418	0.169	0.125	5.659006
6	358	18:07:46.98	-32:29:20.1	1.739	15.439	0.246	0.064	3.476010
6	598	18:08:28.11	-32:24:58.7	1.731	18.033	0.326	0.158	2.457010
6	1214	18:08:34.60	-32:12:28.4	1.683	16.958	0.431	0.242	5.688314

6	1517	18:07:56.87	-32:06:12.5	1.335	17.511	0.102	0.078	6.417924
7	299	18:08:51.59	-32:23:13.2	1.504	18.265	0.087	0.078	4.048338
7	605	18:09:14.45	-32:10:42.7	1.865	17.022	0.383	0.324	4.259042
7	1494	18:08:52.25	-31:42:44.0	1.410	17.626	0.134	0.113	3.341994
8	430	18:23:30.17	-22:03:23.6	2.026	16.850	0.416	0.076	3.499018
8	829	18:23:23.13	-21:54:38.5	1.969	17.260	0.239	0.198	4.084482
10	1924	18:20:06.01	-22:09:22.3	1.951	17.836	0.215	0.111	4.128718
10	2053	18:20:00.77	-22:07:06.5	1.778	16.923	0.311	0.286	3.729120
11	1231	18:20:54.55	-22:21:07.1	1.910	16.945	0.349	0.245	3.733986
11	1934	18:21:22.82	-22:03:02.7	2.119	16.015	0.289	0.106	11.554690
12	1664	18:16:26.54	-24:00:08.6	2.071	17.492	0.180	0.121	2.812648
12	2249	18:16:22.47	-23:50:50.8	1.909	17.937	0.177	0.109	4.133296
12	3118	18:15:57.17	-23:35:39.6	2.105	17.756	0.215	0.111	2.731754
13	515	18:16:54.03	-24:16:52.7	2.179	17.315	0.209	0.198	2.280115
13	643	18:17:21.43	-24:15:08.1	2.228	18.266	0.429	0.229	2.543559
13	748	18:16:47.11	-24:11:53.1	2.477	17.513	0.184	0.085	3.086584
14	748	17:46:47.93	-23:24:30.5	2.054	16.809	0.270	0.116	3.205315
14	842	17:46:34.66	-23:22:50.8	2.108	15.063	0.281	0.123	4.724715
14	1246	17:47:16.93	-23:16:39.8	2.224	16.485	0.256	0.092	10.525937
14	1360	17:46:51.72	-23:14:51.2	2.042	18.241	0.278	0.107	5.335997
14	2296	17:47:19.49	-23:03:42.5	2.428	15.460	0.240	0.056	2.429135
14	3223	17:47:01.51	-22:53:10.2	2.043	17.372	0.307	0.168	2.697653
14	3755	17:46:38.18	-22:43:40.9	1.996	17.495	0.317	0.237	2.063695
15	529	17:47:50.68	-23:25:54.5	2.122	17.324	0.371	0.172	4.172854
15	631	17:48:16.06	-23:25:22.9	2.125	17.695	0.285	0.228	2.886554
15	851	17:48:12.09	-23:21:51.4	2.277	17.754	0.385	0.191	3.268354
15	1341	17:47:50.79	-23:15:13.1	2.424	17.552	0.198	0.116	2.767438
15	2256	17:48:13.84	-23:02:45.3	2.297	17.944	0.376	0.270	2.562922
16	147	18:10:03.80	-26:44:29.4	2.035	18.238	0.190	0.094	7.611000
16	443	18:09:55.54	-26:40:37.0	2.073	17.613	0.338	0.229	2.515553
16	722	18:09:58.67	-26:36:52.8	2.165	17.419	0.406	0.268	5.064416
16	2304	18:09:58.50	-26:19:18.5	1.821	16.691	0.356	0.137	3.572162
16	3066	18:09:45.75	-26:10:33.8	1.977	17.956	0.287	0.179	4.327591
17	417	18:11:10.05	-26:34:35.0	1.639	16.783	0.369	0.235	2.958341
17	1576	18:10:51.97	-26:21:58.3	1.902	17.489	0.418	0.125	3.480961
17	1577	18:10:58.42	-26:22:06.7	2.019	16.847	0.181	0.130	20.532350
17	2366	18:11:07.56	-26:11:28.4	1.663	17.709	0.150	0.136	2.771794
17	4107	18:11:07.22	-25:49:57.8	1.863	16.939	0.367	0.153	3.584156
18	667	18:06:37.36	-27:33:42.9	2.116	16.079	0.172	0.074	9.504011
18	1201	18:06:42.52	-27:28:03.3	1.553	17.341	0.274	0.207	3.936500
18	2492	18:06:38.20	-27:17:03.5	1.509	17.265	0.254	0.101	3.187028
18	3232	18:07:07.99	-27:09:23.8	1.668	16.559	0.207	0.117	2.345478

18	3834	18:06:33.83	-27:03:35.0	1.649	17.338	0.153	0.082	4.064586
18	3942	18:06:43.70	-27:02:38.1	1.595	16.204	0.259	0.242	4.271732
18	4093	18:07:25.56	-27:01:43.0	1.854	17.096	0.332	0.229	3.373929
18	4246	18:06:59.39	-27:00:14.5	1.552	17.062	0.380	0.267	5.194025
18	4368	18:07:03.12	-26:59:28.2	1.596	17.437	0.213	0.141	2.582868
19	3463	18:07:44.88	-27:02:14.3	2.022	17.794	0.310	0.207	2.165127
19	4115	18:08:31.28	-26:56:27.2	1.699	17.174	0.325	0.244	2.022135
20	508	17:59:17.21	-29:15:46.0	1.784	16.925	0.346	0.246	6.437626
20	625	17:59:11.17	-29:14:26.7	1.713	16.759	0.267	0.160	2.156676
20	726	17:59:12.62	-29:13:58.6	1.620	17.047	0.359	0.323	3.220336
20	764	17:59:37.56	-29:13:20.1	1.788	17.347	0.308	0.134	4.828995
20	1218	17:59:32.08	-29:09:34.2	1.773	17.572	0.303	0.250	4.204415
20	3228	17:59:39.47	-28:49:45.6	2.033	15.511	0.301	0.084	2.761122
20	3507	17:59:23.84	-28:47:26.0	1.637	17.043	0.358	0.250	2.431410
20	3703	17:59:09.40	-28:45:47.1	2.053	18.174	0.200	0.182	7.134314
20	3831	17:59:26.04	-28:44:13.9	1.958	16.494	0.121	0.071	3.034756
20	4260	17:59:36.54	-28:40:51.1	1.833	17.474	0.214	0.107	4.127868
20	5428	17:58:56.59	-28:29:28.5	2.034	17.265	0.269	0.198	2.185926
21	564	18:00:46.24	-29:15:53.4	1.970	17.238	0.365	0.255	2.753914
21	1563	18:00:34.98	-29:07:43.6	1.954	15.966	0.184	0.032	28.799444
21	1588	18:00:43.62	-29:08:08.8	1.733	15.282	0.312	0.224	3.740300
21	2360	18:00:22.92	-29:01:28.2	1.543	16.283	0.520	0.176	3.589142
21	2601	18:00:06.28	-29:00:11.0	1.579	17.763	0.230	0.132	3.180098
21	2750	18:00:35.67	-28:58:56.2	1.534	17.480	0.325	0.255	2.220600
21	3596	18:00:09.93	-28:52:40.9	2.038	18.247	0.360	0.334	4.252551
21	4732	18:00:33.33	-28:45:29.7	2.181	17.291	0.223	0.062	2.871256
21	6233	18:00:03.29	-28:33:32.7	2.488	16.801	0.415	0.141	2.923352
21	6795	18:00:09.54	-28:29:11.3	1.806	16.978	0.351	0.203	5.214180
21	7051	18:00:42.73	-28:27:10.0	1.867	17.868	0.323	0.204	2.701986
21	7356	18:00:25.77	-28:24:37.8	1.944	16.954	0.316	0.307	4.641814
22	10	17:56:27.07	-31:15:31.6	1.988	17.542	0.285	0.196	4.378102
22	114	17:57:20.34	-31:14:52.1	2.215	17.198	0.392	0.203	4.809705
22	222	17:56:23.41	-31:13:10.8	2.259	17.795	0.155	0.057	11.372206
22	1335	17:57:12.80	-31:01:58.1	1.774	17.769	0.405	0.211	2.119743
22	2938	17:56:28.02	-30:47:05.7	1.761	16.769	0.240	0.113	4.996538
23	293	17:57:23.92	-31:36:32.2	2.103	18.642	0.208	0.083	5.482078
23	1425	17:57:34.18	-31:23:01.8	2.346	17.864	0.274	0.241	2.203385
23	1695	17:57:38.45	-31:19:27.1	2.601	17.894	0.276	0.219	2.837150
23	3566	17:57:44.81	-30:58:12.4	2.299	18.165	0.446	0.227	2.023772
23	3832	17:57:38.48	-30:55:07.3	2.678	15.592	0.481	0.085	36.548702
24	1797	17:53:38.44	-32:55:12.2	2.144	17.542	0.350	0.227	8.378970
24	2166	17:53:03.75	-32:49:24.8	2.029	16.710	0.304	0.147	6.788291

24	2463	17:53:04.50	-32:45:05.9	2.564	15.956	0.266	0.075	2.846186
25	425	17:54:39.82	-33:11:54.2	2.022	17.896	0.357	0.308	2.807364
25	2256	17:54:16.80	-32:37:23.3	1.886	17.655	0.446	0.233	3.888740
25	2800	17:54:22.11	-32:28:52.9	1.867	17.709	0.234	0.117	4.863817
25	2836	17:53:59.11	-32:28:01.3	1.870	17.235	0.357	0.255	2.113844
26	572	17:46:59.47	-35:19:42.8	2.003	16.379	0.215	0.084	13.478680
26	946	17:46:58.93	-35:15:02.0	1.814	17.455	0.287	0.190	2.131286
26	1376	17:47:03.47	-35:09:54.2	1.838	17.619	0.348	0.312	2.009605
26	3703	17:47:10.75	-34:43:40.4	1.682	15.740	0.116	0.029	2.620312
26	3875	17:47:08.15	-34:43:16.5	1.732	17.322	0.117	0.076	2.396786
26	4375	17:47:45.91	-34:36:39.6	2.014	18.062	0.197	0.122	2.961308
26	4395	17:46:46.31	-34:36:26.1	2.021	17.902	0.171	0.125	3.688354
27	323	17:48:23.02	-35:32:00.8	1.524	16.950	0.120	0.051	2.038052
27	646	17:48:20.08	-35:26:48.3	1.599	17.457	0.357	0.325	3.404542
27	1512	17:48:30.63	-35:15:20.6	1.594	16.877	0.312	0.284	3.744963
27	1587	17:47:58.47	-35:13:20.4	1.638	17.604	0.290	0.132	2.221579
27	2801	17:47:57.32	-34:55:17.3	1.639	17.837	0.257	0.127	4.287232
28	974	17:46:33.81	-36:56:26.9	1.694	17.141	0.181	0.059	3.625968
28	1355	17:46:59.43	-36:43:51.2	1.735	18.333	0.271	0.222	2.050652
29	491	17:47:48.95	-37:21:59.4	1.596	16.120	0.386	0.212	3.137304
29	943	17:47:53.46	-37:11:14.8	1.603	17.413	0.226	0.125	6.781612
29	1001	17:48:13.64	-37:10:05.6	1.461	16.225	0.303	0.238	3.450851
29	1063	17:47:57.24	-37:08:22.1	1.574	16.961	0.398	0.165	2.255049
29	1149	17:48:43.11	-37:06:33.9	1.812	17.158	0.220	0.207	8.651742
29	1755	17:48:12.65	-36:52:44.1	1.949	16.930	0.463	0.208	10.219748
30	983	18:01:12.34	-29:08:57.4	1.968	16.868	0.101	0.075	36.279276
30	1034	18:01:51.72	-29:08:47.0	1.971	17.219	0.304	0.153	3.515654
30	1558	18:00:57.01	-29:03:37.4	1.763	16.068	0.139	0.043	5.385688
30	2126	18:01:53.58	-28:59:19.6	1.889	17.735	0.396	0.313	2.539593
30	2158	18:01:07.93	-28:58:25.6	1.642	16.387	0.390	0.293	2.205462
30	2508	18:01:24.79	-28:55:21.9	1.791	17.463	0.311	0.157	5.518564
30	3167	18:01:48.86	-28:51:10.8	1.615	17.629	0.160	0.111	3.254480
30	5566	18:01:11.19	-28:32:38.6	1.661	17.393	0.193	0.134	4.206418
30	5978	18:00:57.98	-28:29:09.2	1.774	16.501	0.173	0.067	10.134768
31	399	18:01:53.58	-28:59:19.7	1.831	17.735	0.389	0.314	2.539666
31	2277	18:02:26.01	-28:34:28.9	2.109	17.576	0.311	0.179	3.181014
31	2670	18:02:30.81	-28:29:58.1	1.951	17.559	0.412	0.260	2.312017
31	2793	18:01:53.97	-28:27:47.4	1.789	17.137	0.201	0.105	6.405328
31	3308	18:02:27.26	-28:23:22.3	1.777	17.224	0.365	0.180	2.686944
31	4092	18:02:49.03	-28:16:33.3	1.659	17.698	0.295	0.231	3.067622
31	4328	18:02:25.28	-28:13:40.1	1.593	17.387	0.104	0.070	7.872418
31	4787	18:02:49.76	-28:09:59.3	1.556	17.561	0.420	0.304	3.079226

32	926	18:03:26.66	-28:54:40.6	1.544	17.382	0.107	0.053	13.887762
32	1504	18:03:37.95	-28:48:24.6	1.680	17.251	0.273	0.167	6.526399
32	1928	18:03:54.07	-28:43:54.9	1.738	16.620	0.383	0.251	4.992396
32	2053	18:03:34.10	-28:41:56.9	1.686	17.126	0.172	0.111	7.414870
32	3061	18:03:17.72	-28:31:15.5	2.076	17.038	0.266	0.110	5.346271
32	3753	18:03:19.86	-28:23:36.5	1.752	17.151	0.184	0.054	9.886980
32	4589	18:03:56.25	-28:14:43.9	1.569	16.890	0.153	0.087	5.627108
33	547	18:05:36.60	-29:13:14.3	1.840	17.417	0.383	0.170	3.463207
33	686	18:05:26.29	-29:11:57.4	1.612	17.791	0.162	0.097	4.095290
33	1629	18:05:21.08	-28:59:58.8	1.760	17.658	0.305	0.162	2.058984
33	2278	18:05:26.10	-28:52:17.1	1.663	18.171	0.396	0.165	2.013036
33	3188	18:05:45.64	-28:42:47.6	1.867	17.858	0.265	0.191	6.148376
34	420	17:58:18.98	-29:32:57.1	2.097	17.302	0.277	0.139	2.231450
34	793	17:57:50.07	-29:29:10.9	1.857	17.068	0.310	0.200	7.976383
34	1615	17:58:36.95	-29:22:51.7	2.005	17.930	0.376	0.265	2.540265
34	1706	17:58:20.31	-29:22:39.9	1.919	17.476	0.283	0.079	4.267768
34	1951	17:58:35.51	-29:20:59.3	1.838	17.803	0.313	0.295	2.224765
34	2456	17:58:05.20	-29:16:05.0	2.114	17.097	0.248	0.080	8.471958
34	2580	17:58:20.21	-29:14:57.9	1.779	17.759	0.127	0.093	6.439528
34	2823	17:58:33.05	-29:13:31.2	1.583	16.233	0.160	0.045	3.521810
34	2973	17:58:42.81	-29:12:15.3	1.649	16.020	0.369	0.202	3.183053
34	5744	17:58:04.66	-28:53:04.9	2.026	17.878	0.158	0.089	5.301156
35	2440	18:04:06.62	-27:58:54.6	1.793	17.764	0.312	0.198	2.022147
35	2508	18:04:02.60	-27:58:23.6	1.722	14.118	0.210	0.031	21.505206
35	2897	18:04:36.18	-27:54:27.0	2.493	16.517	0.335	0.222	2.453367
35	4121	18:04:27.93	-27:41:05.1	1.864	16.660	0.437	0.248	2.551206
35	4556	18:04:38.36	-27:36:26.2	1.624	17.057	0.200	0.092	4.054498
35	4721	18:04:11.40	-27:33:39.3	1.841	15.595	0.317	0.121	2.759243
36	1929	18:05:47.36	-28:13:03.3	1.910	16.848	0.393	0.173	8.543916
36	3762	18:05:05.62	-28:00:35.3	1.639	16.801	0.128	0.050	2.586147
36	4333	18:05:31.34	-27:57:11.9	1.964	17.726	0.389	0.138	3.928802
36	4493	18:05:51.25	-27:56:20.9	1.701	17.319	0.292	0.249	3.118629
36	4494	18:05:55.08	-27:56:12.2	1.992	17.223	0.330	0.271	2.910082
36	7720	18:05:37.14	-27:36:22.0	1.613	17.819	0.239	0.161	3.115270
37	956	17:52:52.82	-30:18:52.1	2.442	17.944	0.334	0.254	3.262918
37	2068	17:52:22.28	-30:09:18.0	2.722	18.234	0.388	0.296	3.662674
37	2768	17:52:19.88	-30:05:22.0	2.730	17.333	0.391	0.318	5.733310
37	3186	17:52:35.96	-30:02:52.3	3.339	17.570	0.310	0.211	5.098516
37	3240	17:52:05.16	-30:01:32.7	3.122	18.193	0.250	0.199	3.091703
37	4541	17:52:06.26	-29:53:15.8	2.800	16.147	0.435	0.076	2.907292
37	6333	17:52:13.81	-29:40:19.7	2.973	18.570	0.290	0.267	2.943085
37	6549	17:52:52.89	-29:39:27.2	2.724	17.381	0.275	0.164	2.647908

37	7240	17:52:02.98	-29:35:30.7	3.491	17.082	0.300	0.087	2.012917
37	8237	17:52:51.31	-29:30:29.8	2.834	17.937	0.426	0.259	3.955137
38	1003	18:01:29.06	-30:14:16.6	1.901	17.678	0.321	0.236	2.495866
38	1675	18:01:37.77	-30:07:31.4	1.619	17.156	0.343	0.296	2.396601
38	3532	18:01:10.10	-29:46:17.9	1.795	17.420	0.357	0.207	6.338837
38	3758	18:02:00.41	-29:44:30.0	1.634	17.102	0.234	0.076	4.501576
38	4718	18:01:24.01	-29:33:20.9	1.868	16.910	0.330	0.106	4.589060
38	5059	18:01:57.05	-29:30:27.5	2.193	16.816	0.108	0.105	3.617376
39	511	17:56:01.79	-30:08:43.3	2.124	17.210	0.323	0.143	2.220596
39	1893	17:55:08.38	-29:56:48.4	1.872	17.722	0.396	0.146	2.452596
39	2555	17:55:24.39	-29:52:20.7	2.389	17.157	0.288	0.200	2.879248
39	2745	17:55:16.18	-29:50:20.9	2.168	16.717	0.313	0.088	8.139266
39	3008	17:55:31.48	-29:48:50.6	2.772	18.302	0.268	0.154	3.591320
39	4483	17:55:25.33	-29:38:32.6	2.412	18.056	0.245	0.165	4.946640
39	5279	17:55:15.81	-29:32:08.1	1.833	16.698	0.306	0.118	5.776876
39	5315	17:55:37.41	-29:31:44.2	1.905	18.374	0.292	0.180	2.048580
39	6095	17:55:19.90	-29:26:12.8	2.106	17.206	0.388	0.236	2.885993
39	6554	17:56:05.16	-29:23:08.8	2.351	18.098	0.312	0.228	2.144490
40	1732	17:51:09.87	-33:19:16.9	2.229	16.557	0.351	0.250	2.934772
40	1808	17:50:54.17	-33:18:35.6	2.199	17.029	0.370	0.259	2.465588
41	207	17:52:06.31	-33:31:42.0	2.280	16.931	0.440	0.241	9.307920
41	279	17:52:37.85	-33:30:41.5	1.833	18.366	0.196	0.139	2.583558
41	1414	17:52:15.20	-33:14:55.5	2.076	17.974	0.312	0.148	2.544096
41	1593	17:52:35.87	-33:13:14.6	2.074	17.135	0.409	0.225	6.934563
42	872	18:09:09.69	-27:09:24.1	2.014	17.096	0.242	0.120	2.083840
42	875	18:09:11.46	-27:09:32.6	1.852	17.414	0.239	0.110	4.297795
42	1309	18:09:08.77	-27:03:57.7	1.706	16.405	0.446	0.261	4.606988
42	4197	18:09:17.51	-26:26:31.4	2.056	17.903	0.416	0.158	2.161317
42	4324	18:08:55.48	-26:25:19.7	1.976	15.675	0.373	0.224	2.452289
43	305	17:34:47.64	-27:32:53.8	2.926	18.133	0.267	0.174	6.457909
43	310	17:35:04.55	-27:32:29.1	2.706	18.111	0.348	0.223	6.223798
43	834	17:34:45.85	-27:22:45.7	2.998	18.724	0.349	0.309	2.242491
43	1023	17:35:38.97	-27:19:56.0	2.769	18.727	0.410	0.216	2.140171
43	2852	17:35:40.60	-26:53:12.4	2.654	17.204	0.306	0.263	4.098304
44	2264	17:49:11.53	-30:10:08.3	3.519	18.243	0.152	0.117	3.218736
46	178	18:04:24.67	-30:28:10.5	1.874	16.991	0.311	0.156	3.379805
46	1863	18:04:26.40	-29:42:49.6	1.402	16.447	0.137	0.077	5.429178
46	1982	18:04:46.68	-29:39:41.2	1.796	16.902	0.371	0.227	3.712870
46	2039	18:04:16.65	-29:37:23.5	2.096	15.451	0.401	0.201	2.679111
48	911	17:28:30.26	-39:21:47.3	1.924	16.172	0.376	0.264	3.618835

Table 2: We tabulate the OGLE-II identification, coordinates, apparent magnitudes, relative radii and periods for the gold (top) and silver (bottom) sample RG eclipsing binary pairs identified. More detailed properties can be found in the catalog of Devor (2005) from which these candidates were identified. E_1 is the epoch of the eclipse when the secondary is behind the primary. The star IDs used here are those from the catalog of Devor (2005). The original photometry for these sources can be found on the OGLE-II archive (Udalski *et al.* 1997; Szymanski *et al.* 2005).

Field	ID	e	E_2	t_1 (days)	$\sin i$
3	2325	0.146	2450000.18	0.53	0.934
3	2823	0.016	2449999.60	0.41	0.996
3	2929	0.007	2450002.04	0.41	0.982
3	7715	0.085	2450000.38	0.64	0.978
4	830	0.062	2450002.58	0.91	0.915
4	831	0.071	2450000.26	0.30	0.999
4	1290	0.105	2450003.48	0.45	0.995
5	1889	0.133	2449998.25	0.81	0.985
7	1089	0.049	2450001.36	0.31	1.000
9	132	0.150	2450001.36	0.43	0.947
9	1502	0.008	2450002.67	0.42	0.984
13	1282	0.036	2450000.63	0.99	0.990
14	3912	0.189	2450001.04	0.61	0.974
24	1374	0.310	2450000.38	0.61	0.943
24	2461	0.009	2449990.80	2.25	0.955
30	1600	0.009	2450002.26	0.41	0.977
30	6658	0.061	2450007.81	1.11	0.960
31	631	0.270	2450002.81	0.46	0.981
31	2641	0.022	2450002.04	0.49	0.992
34	1369	0.030	2450000.31	0.79	0.988
34	6500	0.091	2450002.73	0.39	0.996
37	1846	0.048	2450000.90	0.32	0.941
37	6396	0.077	2450002.06	0.72	0.967
37	7093	0.057	2450002.88	0.55	0.985
39	1159	0.160	2450002.16	0.52	0.986
39	1604	0.084	2450000.11	0.32	1.000
40	310	0.293	2450003.46	0.96	0.994
40	621	0.149	2450006.12	0.96	0.953
43	3095	0.015	2450001.83	0.54	0.957
45	1064	0.203	2450087.27	4.99	0.999
45	1155	0.008	2450004.72	0.55	0.997
45	1522	0.054	2450002.05	0.28	0.993

45	2170	0.088	2450009.51	1.86	1.000
47	481	0.091	2450001.98	0.38	0.984
1	1713	0.017	2450003.65	0.25	0.998
1	2513	0.003	2450002.41	0.31	0.896
1	2938	0.205	2449999.27	0.34	0.987
1	3738	0.088	2450000.55	0.30	0.995
1	3846	0.377	2450002.09	0.71	0.999
1	3859	0.131	2450000.92	0.36	0.972
2	892	0.284	2450001.93	0.59	0.965
2	1301	0.059	2450006.32	0.52	0.995
2	1800	0.161	2449999.68	0.22	0.995
2	2542	0.024	2450001.47	0.35	0.973
2	3673	0.450	2450012.14	1.33	1.000
2	3894	0.034	2450003.90	0.36	0.992
2	4754	0.045	2449999.62	0.22	0.995
3	1149	0.043	2450002.60	0.43	0.932
3	1688	0.113	2450002.78	0.30	0.993
3	2195	0.113	2449999.43	0.41	0.912
3	3488	0.141	2450000.73	0.18	1.000
3	3489	0.161	2450000.85	0.27	0.999
3	3547	0.143	2450000.24	0.21	0.988
3	3744	0.103	2450001.63	0.37	0.964
3	6413	0.169	2450005.48	0.87	0.978
3	8222	0.212	2450006.10	0.72	0.983
3	8395	0.088	2449999.98	0.71	0.990
4	1047	0.061	2450001.89	0.21	0.975
4	1120	0.326	2450004.47	1.02	0.941
4	1224	0.340	2450000.85	0.61	0.987
4	1289	0.006	2450000.10	0.30	0.991
4	3707	0.010	2450002.88	0.23	0.983
4	4049	0.056	2450000.30	0.15	0.995
4	4449	0.283	2450002.19	0.39	0.925
4	4564	0.098	2450001.56	0.35	0.987
4	5392	0.043	2450001.82	0.15	0.991
4	6839	0.004	2450000.51	0.24	0.961
4	6905	0.028	2450001.74	0.34	0.981
4	7346	0.128	2450002.42	0.28	0.996
4	8604	0.003	2449999.09	0.27	0.998
5	5124	0.074	2450001.96	0.30	0.995
6	358	0.585	2450001.97	0.27	0.993
6	598	0.063	2450000.40	0.25	0.995
6	1214	0.191	2450003.06	0.77	0.951

6	1517	0.005	2450001.71	0.21	1.000
7	299	0.037	2449999.88	0.11	1.000
7	605	0.134	2450002.56	0.52	0.998
7	1494	0.036	2450001.95	0.14	0.997
8	430	0.149	2450001.26	0.46	0.969
8	829	0.025	2450000.33	0.31	0.995
10	1924	0.095	2450000.11	0.28	1.000
10	2053	0.076	2450002.24	0.37	0.990
11	1231	0.017	2450004.38	0.41	0.995
11	1934	0.077	2450004.78	1.06	0.986
12	1664	0.007	2450001.58	0.16	0.999
12	2249	0.029	2450002.26	0.23	1.000
12	3118	0.054	2450002.24	0.19	1.000
13	515	0.494	2450000.50	0.15	0.991
13	643	0.242	2450001.77	0.35	0.994
13	748	0.005	2450000.69	0.18	0.996
14	748	0.187	2450000.90	0.28	1.000
14	842	0.097	2450006.78	0.42	0.981
14	1246	0.533	2450009.26	0.86	1.000
14	1360	0.159	2450002.40	0.47	1.000
14	2296	0.075	2450002.07	0.19	0.995
14	3223	0.031	2450001.18	0.26	0.991
14	3755	0.165	2450001.69	0.21	0.971
15	529	0.270	2449999.35	0.49	0.983
15	631	0.027	2450000.15	0.26	1.000
15	851	0.000	2450001.61	0.40	0.994
15	1341	0.014	2450001.42	0.17	0.995
15	2256	0.212	2450002.68	0.31	0.997
16	147	0.006	2450003.99	0.46	0.996
16	443	0.099	2449999.72	0.27	0.993
16	722	0.010	2450002.17	0.64	0.946
16	2304	0.081	2450002.34	0.40	0.981
16	3066	0.180	2450002.01	0.39	0.998
17	417	0.047	2450000.36	0.35	0.981
17	1576	0.446	2450000.33	0.46	1.000
17	1577	0.023	2450013.98	1.18	0.999
17	2366	0.027	2450000.55	0.13	0.996
17	4107	0.018	2450000.12	0.42	0.985
18	667	0.751	2450006.28	0.52	1.000
18	1201	0.123	2449999.32	0.34	0.983
18	2492	0.078	2450003.06	0.26	1.000
18	3232	0.064	2450000.77	0.15	0.980

18	3834	0.011	2450001.89	0.20	0.998
18	3942	0.077	2450004.24	0.35	0.989
18	4093	0.098	2449998.71	0.36	0.994
18	4246	0.115	2450006.97	0.62	0.980
18	4368	0.014	2450002.51	0.17	0.993
19	3463	0.075	2450000.00	0.21	0.995
19	4115	0.017	2450001.19	0.21	0.997
20	508	0.236	2450006.39	0.70	0.978
20	625	0.038	2450002.39	0.18	0.981
20	726	0.106	2450000.04	0.36	0.933
20	764	0.098	2450006.14	0.47	0.990
20	1218	0.009	2450000.64	0.41	0.994
20	3228	0.069	2450001.66	0.26	0.976
20	3507	0.006	2450001.63	0.28	0.973
20	3703	0.027	2450003.29	0.45	1.000
20	3831	0.032	2449999.51	0.12	0.998
20	4260	0.065	2450002.41	0.28	1.000
20	5428	0.056	2450003.17	0.19	0.993
21	564	0.031	2450001.79	0.32	0.984
21	1563	0.041	2450022.50	1.68	1.000
21	1588	0.007	2450001.60	0.37	0.941
21	2360	0.304	2450000.75	0.57	0.909
21	2601	0.066	2450000.03	0.23	0.987
21	2750	0.009	2450002.00	0.23	0.996
21	3596	0.034	2450003.44	0.49	1.000
21	4732	0.715	2450001.35	0.20	0.995
21	6233	0.021	2450001.27	0.39	0.998
21	6795	0.052	2450003.61	0.58	0.998
21	7051	0.070	2450000.94	0.28	0.999
21	7356	0.031	2450000.90	0.46	0.964
22	10	0.160	2450000.71	0.40	0.979
22	114	0.238	2450000.75	0.60	0.988
22	222	0.046	2450007.33	0.56	1.000
22	1335	0.020	2450001.18	0.27	0.958
22	2938	0.082	2450002.79	0.38	0.992
23	293	0.118	2450004.27	0.36	0.999
23	1425	0.039	2449999.64	0.19	0.987
23	1695	0.018	2449998.85	0.25	0.997
23	3566	0.130	2450000.91	0.29	0.984
23	3832	0.042	2450036.01	5.55	0.983
24	1797	0.422	2450007.07	0.93	0.985
24	2166	0.234	2449999.78	0.65	0.978

24	2463	0.001	2450002.76	0.24	0.991
25	425	0.031	2450003.26	0.32	1.000
25	2256	0.309	2450003.19	0.55	0.972
25	2800	0.069	2450001.64	0.36	1.000
25	2836	0.084	2450001.06	0.24	0.962
26	572	0.089	2450004.20	0.92	0.995
26	946	0.040	2450000.45	0.19	0.990
26	1376	0.001	2449999.56	0.22	0.997
26	3703	0.319	2450001.69	0.10	0.999
26	3875	0.003	2450001.59	0.09	1.000
26	4375	0.001	2450002.85	0.19	0.993
26	4395	0.002	2450001.02	0.20	0.999
27	323	0.117	2450000.94	0.08	0.998
27	646	0.012	2450000.57	0.38	0.968
27	1512	0.034	2450000.35	0.37	0.999
27	1587	0.578	2450001.80	0.20	0.992
27	2801	0.079	2450004.85	0.35	0.992
28	974	0.009	2450001.45	0.21	1.000
28	1355	0.005	2450001.30	0.18	0.998
29	491	0.396	2450002.76	0.38	0.931
29	943	0.085	2450008.30	0.49	0.999
29	1001	0.002	2450002.67	0.33	0.992
29	1063	0.013	2450001.85	0.28	0.979
29	1149	0.071	2450001.20	0.60	0.980
29	1755	0.186	2450005.32	1.46	0.929
30	983	0.084	2450024.31	1.17	0.999
30	1034	0.240	2450000.80	0.34	0.996
30	1558	0.431	2450001.29	0.24	0.996
30	2126	0.215	2450000.72	0.32	0.993
30	2158	0.104	2449999.72	0.27	0.990
30	2508	0.080	2450002.46	0.54	0.993
30	3167	0.034	2449999.87	0.17	0.997
30	5566	0.015	2450002.92	0.26	1.000
30	5978	0.140	2450009.17	0.56	1.000
31	399	0.297	2450002.57	0.31	0.989
31	2277	0.039	2450001.96	0.31	0.999
31	2670	0.034	2450000.14	0.30	0.998
31	2793	0.065	2450001.42	0.41	0.996
31	3308	0.020	2450000.84	0.31	0.983
31	4092	0.207	2450002.18	0.29	0.970
31	4328	0.025	2450011.57	0.26	1.000
31	4787	0.276	2450002.92	0.41	0.986

32	926	0.002	2450008.44	0.47	1.000
32	1504	0.062	2450003.01	0.57	0.998
32	1928	0.063	2450000.06	0.60	0.945
32	2053	0.009	2450005.37	0.41	0.999
32	3061	0.016	2450000.14	0.45	0.996
32	3753	0.045	2449995.62	0.58	1.000
32	4589	0.068	2449997.85	0.27	0.999
33	547	0.198	2450002.33	0.42	0.984
33	686	0.001	2450002.17	0.21	1.000
33	1629	0.009	2450000.96	0.20	0.992
33	2278	0.119	2450001.35	0.25	0.981
33	3188	0.140	2450003.61	0.52	0.998
34	420	0.087	2450002.23	0.20	0.993
34	793	0.143	2449997.29	0.78	0.963
34	1615	0.059	2450002.31	0.30	0.988
34	1706	0.045	2450000.92	0.38	0.990
34	1951	0.004	2450000.78	0.22	0.997
34	2456	0.092	2450003.99	0.67	0.995
34	2580	0.030	2450002.19	0.26	1.000
34	2823	0.127	2450001.38	0.18	0.999
34	2973	0.058	2450000.71	0.37	0.958
34	5744	0.018	2450002.74	0.27	1.000
35	2440	0.214	2450001.24	0.20	0.999
35	2508	0.066	2450015.41	1.44	0.999
35	2897	0.010	2450000.72	0.26	0.996
35	4121	0.045	2450001.93	0.35	0.985
35	4556	0.005	2449998.35	0.26	0.995
35	4721	0.300	2450000.12	0.28	0.982
36	1929	0.108	2450001.57	1.06	0.975
36	3762	0.822	2450000.63	0.11	1.000
36	4333	0.015	2450001.79	0.49	1.000
36	4493	0.010	2450000.32	0.29	0.996
36	4494	0.007	2450000.33	0.31	0.998
36	7720	0.183	2450003.00	0.24	1.000
37	956	0.127	2450001.54	0.35	0.999
37	2068	0.021	2449999.81	0.45	1.000
37	2768	0.290	2450000.55	0.71	0.963
37	3186	0.113	2450003.36	0.50	0.989
37	3240	0.033	2449999.55	0.25	0.998
37	4541	0.255	2450003.12	0.40	0.957
37	6333	0.006	2450000.15	0.27	0.995
37	6549	0.033	2449999.94	0.23	0.994

37	7240	0.043	2450000.94	0.19	0.999
37	8237	0.176	2450003.66	0.53	0.990
38	1003	0.092	2450002.94	0.25	0.986
38	1675	0.065	2450000.27	0.26	0.992
38	3532	0.395	2450002.55	0.72	0.985
38	3758	0.011	2450000.43	0.34	0.990
38	4718	0.102	2450002.50	0.48	0.982
38	5059	0.081	2450002.76	0.12	0.997
39	511	0.084	2450000.16	0.23	0.984
39	1893	0.124	2450000.19	0.31	1.000
39	2555	0.069	2449999.00	0.26	0.990
39	2745	0.041	2450001.87	0.81	0.990
39	3008	0.043	2450001.65	0.31	0.995
39	4483	0.202	2450001.10	0.39	0.997
39	5279	0.000	2450001.24	0.56	0.971
39	5315	0.408	2450001.96	0.19	1.000
39	6095	0.241	2450002.80	0.35	0.972
39	6554	0.040	2450001.05	0.21	1.000
40	1732	0.003	2450001.15	0.33	0.987
40	1808	0.096	2450000.97	0.29	0.951
41	207	0.319	2450006.21	1.29	0.974
41	279	0.164	2450001.33	0.16	1.000
41	1414	0.099	2450003.28	0.25	0.986
41	1593	0.366	2450005.00	0.89	0.970
42	872	0.043	2450002.10	0.16	0.997
42	875	0.035	2450000.46	0.33	0.993
42	1309	0.292	2449999.94	0.63	0.908
42	4197	0.031	2449999.61	0.28	0.964
42	4324	0.019	2450000.87	0.29	0.974
43	305	0.073	2450005.41	0.55	0.994
43	310	0.207	2450004.46	0.69	1.000
43	834	0.087	2450001.81	0.25	0.992
43	1023	0.189	2450000.19	0.28	0.977
43	2852	0.010	2450002.65	0.40	0.998
44	2264	0.014	2450001.75	0.16	0.999
46	178	0.044	2449999.81	0.33	1.000
46	1863	0.139	2450005.16	0.24	1.000
46	1982	0.148	2450000.30	0.44	0.993
46	2039	0.041	2450000.66	0.33	0.937
48	911	0.093	2450002.22	0.43	0.988